



Politecnico
di Bari

Repository Istituzionale dei Prodotti della Ricerca del Politecnico di Bari

Slope instability processes in intensely fissured clays: case histories in the Southern Apennines

This is a post print of the following article

Original Citation:

Slope instability processes in intensely fissured clays: case histories in the Southern Apennines / Cotecchia, Federica; Vitone, Claudia; Santaloia, F; Pedone, G; Bottiglieri, Osvaldo. - In: LANDSLIDES. - ISSN 1612-510X. - 12:5(2015), pp. 877-893. [10.1007/s10346-014-0516-7]

Availability:

This version is available at <http://hdl.handle.net/11589/1394> since: 2022-06-22

Published version

DOI:10.1007/s10346-014-0516-7

Terms of use:

(Article begins on next page)

Landslides

SLOPE INSTABILITY PROCESSES IN INTENSELY FISSURED CLAYS: CASE HISTORIES IN THE SOUTHERN APENNINES

--Manuscript Draft--

Manuscript Number:	LASL-794R2
Full Title:	SLOPE INSTABILITY PROCESSES IN INTENSELY FISSURED CLAYS: CASE HISTORIES IN THE SOUTHERN APENNINES
Article Type:	Original Paper
Corresponding Author:	CLAUDIA VITONE BARI, ITALY
Corresponding Author Secondary Information:	
Corresponding Author's Institution:	
Corresponding Author's Secondary Institution:	
First Author:	FEDERICA COTECCHIA
First Author Secondary Information:	
Order of Authors:	FEDERICA COTECCHIA CLAUDIA VITONE FRANCESCA SANTALIOIA GIUSEPPE PEDONE OSVALDO BOTTIGLIERI
Order of Authors Secondary Information:	
Abstract:	<p>In slopes formed by tectonized clayey turbidites, the soil fissuring recurrently influences the hydro-mechanical soil properties, determining an impoverishment in strength and an increase in permeability of the slope, that make them predisposing factors of landsliding. This paper presents three case histories of slopes within tectonized clayey turbidites that are representative of several others in the Southern Apennines and, more widely, in the southern Mediterranean. The paper reports a novel attempt to connect tightly the slope geomorphological and hydro-mechanical features to the slope geological history, through an introductory presentation of the geological setting and history of the chain where the slopes occur. The slopes, location of very slow landslides, have been reconstructed based upon field surveys and investigations, multi-aerial photo-interpretation, laboratory testing, monitoring and numerical modelling. Furthermore, novel is the attempt to present, all together, the behaviour of the soils involved in the three landslide case studies, in the light of the mechanical modelling approach to fissured clays recently presented in the literature.</p>

1 SLOPE INSTABILITY PROCESSES IN INTENSELY FISSURED CLAYS: CASE HISTORIES IN THE
2 SOUTHERN APENNINES

3
4 Federica Cotecchia*, Claudia Vitone*, Francesca Santaloia^o, Giuseppe Pedone* and Osvaldo Bottiglieri*

5 * Technical University of Bari, Bari, ITALY

6 ^o IRPI-CNR, U.O.S. Bari, ITALY

7
8
9
10 Federica Cotecchia, PhD, full professor

11 federica.cotecchia@poliba.it

12
13
14
15
16 Claudia Vitone, PhD, lecturer

17 claudia.vitone@poliba.it

18
19
20
21
22 Francesca Santaloia, PhD, lecturer

23 f.santaloia@ba.irpi.cnr.it

24
25
26
27 Giuseppe Pedone, PhD

28 giuseppe.pedone@poliba.it

29
30
31
32
33 Osvaldo Bottiglieri, PhD

34 osvaldo.bottiglieri@poliba.it

35
36
37
38
39
40
41 Corresponding author:

42
43 Claudia Vitone, Technical University of Bari, Bari, Italy

44 email: claudia.vitone@poliba.it

45
46
47 tel. (+39)3391610977

48
49
50
51
52
53
54
55
56
57
58
59
60
61
62
63
64
65

NOTATION LIST

1	
2	A Activity
3	A-B-C: source, channel and accumulation zones of Vadoncello landslides
4	A-C-C9-F-G-L: labels for Pisciole landslide bodies
5	A-F <i>in-situ</i> soil complexes within Vadoncello slope
6	BENT bentonite clay
7	c' cohesion intercept
8	CF Clay Fraction
9	C_k permeability change index
10	e void ratio
11	FAE Faeto Flysch
12	F-ID Fissuring IDentity
13	G-I landslide soil complexes within Vadoncello slope
14	ICL Intrinsic Compression Line
15	INCL* Isotropic Normal Consolidation Line of the reconstituted clay
16	k_s saturated permeability
17	N Numidian Flysch
18	p' mean effective stress
19	p'_e equivalent mean effective stress on the INCL*
20	p'_y mean effective stress at yield in isotropic compression
21	PD Paola Doce Formation
22	PD1 lower unit of Paola Doce Formation
23	PD2 upper unit of Paola Doce Formation
24	PI Pisciole hillslope
25	PI Plasticity Index
26	R overconsolidation ratio: p'_y / p'
27	REV Representative Element Volume
28	RF Red Flysch
29	SBS State Boundary Surface of natural clay
30	SBS* State Boundary Surface of reconstituted clay
31	SCM Santa Croce di Magliano slopes
32	SEN Vadoncello slope
33	SF Sand Fraction
34	S_σ stress sensitivity ratio: p'_y / p'_e
35	USCS Unified Soil Classification System
36	v specific volume
37	ε_v^p plastic volumetric strain
38	ϕ_{cs}^* critical state friction angle of the reconstituted clay
39	ϕ_{cs}' critical state friction angle of the natural clay
40	ϕ'_m mobilised friction angle
41	ϕ'_{peak} friction angle at peak for natural clay
42	$\phi'_{post-peak}$ friction angle at post-peak for natural clay
43	ϕ'_r residual friction angle
44	
45	
46	
47	
48	
49	
50	
51	
52	
53	
54	
55	
56	
57	
58	
59	
60	
61	
62	
63	
64	
65	

1
2 SLOPE INSTABILITY PROCESSES IN INTENSELY FISSURED CLAYS: CASE HISTORIES IN THE
3
4 SOUTHERN APENNINES

5
6 F. Cotecchia*, C. Vitone*, F. Santaloia°, G. Pedone* and O. Bottiglieri*

7
8 * Technical University of Bari, Bari, ITALY

9
10 ° IRPI-CNR, U.O.S. Bari, ITALY

11
12
13
14 ABSTRACT

15
16 In slopes formed by tectonized clayey turbidites, the soil fissuring recurrently influences the hydro-mechanical soil
17
18 properties, determining an impoverishment in strength and an increase in permeability of the slope, that make them
19
20 predisposing factors of landsliding. This paper presents three case histories of slopes within tectonized clayey
21
22 turbidites that are representative of several others in the Southern Apennines and, more widely, in the southern
23
24 Mediterranean. The paper reports a novel attempt to connect tightly the slope geomorphological and hydro-mechanical
25
26 features to the slope geological history, through an introductory presentation of the geological setting and history of
27
28 the chain where the slopes occur. The slopes, location of very slow landslides, have been reconstructed based upon
29
30 field surveys and investigations, multi-aerial photo-interpretation, laboratory testing, monitoring and numerical
31
32 modelling. Furthermore, novel is the attempt to present, all together, the behaviour of the soils involved in the three
33
34 landslide case studies, in the light of the mechanical modelling approach to fissured clays recently presented in the
35
36 literature.

37
38
39
40
41
42 KEYWORDS: fissured clays, slow landslides, mechanical and hydraulic soil properties, tectonized flysch
43
44
45
46
47
48
49
50
51
52
53
54
55
56
57
58
59
60
61
62
63
64
65

1
2 INTRODUCTION
3

4 The soils outcropping within chain areas, namely areas that have been location of orogenesis, have generally
5 experienced severe tectonic processes. This is the case of the soils within the Apennines in southern Italy, a chain area
6 part of one of the most important and still active thrust systems in the Mediterranean. The present paper focuses on
7 instability processes that recur in tectonized clay slopes across this chain and on the slope factors predisposing to
8 instability.
9

10 The tectonized soil sequences are classified, since the seventies, as “structurally complex formations” (e.g., Croce
11 1971; AGI 1979), due to their lithological variability, heterogeneous consistency and fissuring. Several research
12 studies (Croce 1971; Pellegrino and Picarelli 1982; Fenelli et al. 1982; Santaloia et al. 2001; Cotecchia et al. 2007)
13 have shown that the soils part of structurally complex formations exhibit very low shear strength, by comparison with
14 that of soils of the same composition, but possessing a structure that has not experienced severe disturbance due to
15 tectonics. Consequently, the poor shear strength of the tectonized soils represents a common internal factor (Terzaghi
16 1950) predisposing the slopes to failure in the area of reference in the present paper. Hence, the mechanical
17 characterisation of the tectonized soils is crucial for landslide hazard assessments.
18

19 The inhomogeneities and the fissuring of tectonized soils introduce critical difficulties in both investigation and
20 interpretation of their behaviour (e.g., Calabresi and Manfredini 1973; Cicolella and Picarelli 1990; Cotecchia and
21 Santaloia 2003; Picarelli and Olivares 2004; Airò Farulla et al. 2010). Overcoming these difficulties has been the goal
22 of a research carried out at the Technical University of Bari, aimed in particular at characterising the influence of
23 fissuring on the hydro-mechanical properties of tectonized clays (Cotecchia and Santaloia 2003; Cotecchia and Vitone
24 2011; Vitone and Cotecchia 2011; Vitone et al. 2013a, b). In this paper, the main results of the research are recalled,
25 first to show how the basic features of the hydro-mechanics of fissured clays can be modelled by means of a single
26 framework. As second, it is shown how this framework proves that the hydro-mechanical properties of fissured clays
27 can predispose slopes to failure.
28

29 In particular, they are discussed the properties of the tectonized clays present in Southern Apennine slopes that are
30 location of very slow landslides, together with the corresponding landslide mechanisms. These have been
31 reconstructed based upon field surveys and investigations, multi-aerial photo-interpretation, laboratory testing,
32 monitoring and numerical modelling. The chosen slopes are representative of several others in the Southern
33
34
35
36
37
38
39
40
41
42
43
44
45
46
47
48
49
50
51
52
53
54
55
56
57
58
59
60
61
62
63
64
65

1 Apennines. They are (Fig. 1): the Vadoncello slope (western sector of the chain), located down the Senerchia village
2 in the upper Sele River Valley; the Pisciola hillslope, located on the right side of the Ofanto River valley, to the West
3 of Melfi (eastern sector of the chain); the Santa Croce di Magliano slopes (eastern sector of the chain).
4

5
6 As first, the paper reports a presentation of the geological setting and history of the chain, in order to connect
7 tightly the current slope geomorphological and hydro-mechanical features to the slope history. Thereafter, the paper
8 reports a novel attempt to show how the behaviour of all the soils involved in the three landslide case studies fits the
9 mechanical modelling cited before. In a wider perspective, the aim of the work is to contribute to the characterisation
10 of the possible landslide mechanisms occurring in landscapes ensued from an intense tectonic history. These
11 landscapes are recurrent in the southern Mediterranean, where landsliding is very diffuse and represents a major
12 problem for socio-economic development.
13
14
15
16
17
18
19
20
21

22 GEOLOGICAL SETTING

23
24 The Italian Southern Apennine is part of the Apennine-Maghrebian chain, important branch of the circum-
25 Mediterranean Alpidic system (Fig. 1). It is a Neogene to Quaternary thrust belt, verging to North-East, located in the
26 hanging wall of a West-directed subduction of the Adriatic-African lithosphere, under the European plate (Malinverno
27 and Ryan 1986; Doglioni 1991). It is bordered, to the East, by the Pliocene-Pleistocene foredeep (Bradano Through)
28 and, to the West, by the Tyrrhenian back-arch basin (Scrocca et al. 2005; Fig. 1).
29
30
31
32
33

34 In particular, the Southern Apennine allochthonous nappes derive from the deformation of basin and platform
35 domains within the passive margin of the Adriatic-African plate (Patacca and Scandone 2007). The geological
36 literature does not provide a single conclusive interpretation of the paleogeographic setting of such passive margin and
37 several evolution models have been proposed (Scrocca et al. 2005). The stratigraphic and structural origin of the
38 slopes under study seem to be best represented by the model shown in Fig. 2 (Ogniben 1969; Pescatore et al. 1999).
39 According to it, the main Mesozoic domains involved in the tectonic evolution were, from the West to the East: the
40 Liguride-Sicilide marine domain of the Liguria-Piedmont Ocean, the Apennine carbonate platform, the Lagonegro-
41 Molise marine basin and the Apulian carbonate platform (Fig. 2a). This paleogeographic setting has evolved since
42 Paleogene, as a consequence of the onset of the Apennine orogenesis (Dewey et al. 1989). The internal sectors of the
43 Lagonegro-Molise basin were piled up into the Apennine chain, during Late Oligocene-Early Miocene, while, to the
44 East, turbiditic and hemipelagic successions were deposited in the Irpinian basin (Fig. 2b, Pescatore and Senatore
45
46
47
48
49
50
51
52
53
54
55
56
57
58
59
60
61
62
63
64
65

1986). These successions were thereafter involved in the piling up (Late Miocene) of the Southern Apennine accretionary prism (Fig. 2; Di Nocera et al. 2006).

As a consequence, the geological units (Fig. 2c) deposited in the internal domain, i.e., the Sicilide Unit, occur in the highest portions of the chain, moving further away from its depositional realm, while those formed in the Irpinian basin, i.e., the Daunia Unit, are located in the lowest and easternmost portion of the chain (Patacca and Scandone 2007). Fig. 2c shows two schematic geological sections and the location of the slopes under study: the Vadoncello slope, SEN, the Pisciolò hillslope, PI, and the Santa Croce di Magliano slopes, SCM.

The soils forming the SEN slopes are turbidites belonging to the Sicilide Unit (Fig. 2). The turbiditic sequences outcropping at PI, part of the Fortore Unit, were formed within the northern sector of the pre-orogenic Lagonegro-Molise basin. The clay-rock sequences at SCM belong to the Daunia Unit, formed in the Irpinian basin (Fig. 2). After their deposition, all these sedimentary successions were folded and faulted during orogenesis and, thereafter, were involved in neotectonic events, often giving rise to disarrayed and fissured clay-rock masses.

In more detail, the SEN soils are varicoloured intensely fissured clays part of the allochthonous Variegated Clay Formation (Upper Cretaceous-Lower Miocene); they are chaotically interbedded with fractured rock masses. The geological map and section of the Vadoncello slope are shown in Fig. 3 and will be discussed later in some detail. The clays are in lateral contact with karst calcareous rocks of the Picentini Mountains (Apennine platform in Fig. 2a), that host an important aquifer (Fig. 4).

Clays and isolated rock masses part of the Paola Doce Formation (PD hereafter; Late Oligocene-Lower Miocene) crop out on the PI hillslope, whose geological map and sections are shown in Fig. 5. This formation overlies the Red Flysch (RF herein) and is locally overlain by the Numidian Flysch (N in the following). The clays are found laminated and fissured, including disarranged rock levels from centimetres to metres thick. As depicted in Fig. 5, two different units, PD1 and PD2, have been distinguished in the PD succession, in relation to the frequency and thickness of the rock intervals and coarse layers, which increase from the lower PD1 to the upper PD2.

The clays outcropping along the SCM slopes (Fig. 6) are part of the Red Flysch (RF; Oligocene-Miocene) and are overlain by the marly limestones of the Faeto Flysch (FAE). Some bentonite layers (BENT) are found at places resting on the RF (Fig. 6).

The brief outline of the geological setting of the slopes under study (Fig. 1) reveals that the interbedding of fractured rock strata within the fissured clays is a common slope feature. The geotechnical characterisation of the three

1 sites, discussed later in the paper, focused mainly on the clay properties, since these represent the weakest and most
2 diffuse lithotype, that controls the slope stability.
3
4
5

6 HYDRO-MECHANICAL BEHAVIOUR OF THE CLAYS FORMING THE SLOPES

7 *A framework of behaviour for fissured clays*

8
9
10 The characterisation of fissured clays has always been a major task for geotechnical research (Terzaghi 1936; Lo
11 1970; AGI 1979; Cicoletta and Picarelli 1990; Marsland 1971; Petley 1984; Fearon and Coop 2000, 2002; Picarelli
12 and Olivares 2004; Hight et al. 2007; Silvestri et al. 2007; Airò Farulla et al. 2010). Recent research has been carried
13 out with the aim of assessing a basic simple framework of the influence of fissuring on the mechanics of clays (e.g.,
14 Cotecchia and Santaloia 2003; Vitone 2005; Cotecchia et al. 2007; Cotecchia and Vitone 2011; Vitone and Cotecchia
15 2011), to be addressed in practice for the prediction of the strength reduction stemming from fissuring. The fissuring
16 features have been codified by means of the characterisation chart in Fig. 7, which accounts for both the lithology and
17 consistency of the soil matrix (categories A and B) and the discontinuity features: fissuring nature (C, D, E),
18 orientation (F) and geometry (G-H-I). Fissuring intensity can be characterised by either the average volume of the clay
19 elements between the fissures (i.e., their bulk dimension), or by their specific surface, i.e., average area of the clay
20 element per unit volume. Through several testing programmes on different clays it has resulted that the categories that
21 influence most the fissured clay behaviour are both the fissuring orientation (from single, F1, to random, F3) and the
22 intensity (I).
23
24
25
26
27
28
29
30
31
32
33
34
35

36 The applicability of continuum mechanics and element testing to characterise the mechanics of clays of fissuring
37 intensity from I6 to I4, has been verified by means of full field measurements, using either the False Relief
38 Stereophotogrammetry method (Desrués and Viggiani 2004; Vitone et al. 2009), or Digital Image Correlation
39 techniques (Vitone et al. 2012, 2013 a, b). These measurements have shown that, within Representative Element
40 Volumes (REV) of I4-I6 clay, with fissuring orientation either F3, or F1/0°-30° (fissure inclination with respect to the
41 horizontal and minimum principal stress), the development of shear bands across the specimen takes place similarly to
42 what observed for unfissured clays. Therefore, for these fissure identities (F-IDs hereafter, see Fig. 7), the element test
43 data can be used according to traditional soil mechanics, as for unfissured clays. For F1/30°-90°, instead, strain
44 localization takes place since small displacements and is controlled by pre-existing fissures, which dominate the
45 response of the specimen and make it far weaker. Hence, the characterisation of fissured clay mechanics may be
46
47
48
49
50
51
52
53
54
55
56
57
58
59
60
61
62
63
64
65

1 formalized using continuum mechanics, but, for F3 and F1/0°-30°, it must be developed with reference to REV's which
2 depend on the F-ID, whereas for F1/30°-90°, the element size is irrelevant and the model must account for a
3 significant strength decrease (strength anisotropy; Vitone et al. 2013 a, b).
4

5
6 The behaviour of fissured clays (of F-IDs indicated in grey in Fig. 7; data from Fearon and Coop 2000, 2002;
7 Cotecchia and Santaloia 2003; Cicolella and Picarelli 1990; Vitone and Cotecchia 2011) has been compared with that
8 of the same clays when reconstituted in the laboratory (Burland 1990; Cotecchia and Chandler 2000) and that of
9 unfissured structured clays (Vitone and Cotecchia 2011; Cotecchia and Vitone 2011). Among these, the reconstituted
10 clay possesses the weakest micro-structure. The framework resulting from this comparison is sketched in Fig. 8, where
11 Fig. 8a refers to compression and Fig. 8b to shear. The compression curve of the fissured clay is found to lie on the left
12 of the Intrinsic Compression Line (ICL, Burland 1990) of the reconstituted clay up to high pressures. Hence, the
13 fissured clay does not enter the so-called structure permitted space (Leroueil and Vaughan 1990), possible only for
14 sensitive unfissured clays (Fig. 8a). Cotecchia and Chandler (2000) introduced, for unfissured clays, the stress
15 sensitivity ratio, $S_{\sigma} = p'_{y}/p^{*}_{e}$ (ratio between the mean effective stress at gross yield in isotropic compression, p'_{y} , and
16 the equivalent pressure on the isotropic normal consolidation line of the reconstituted clay, p^{*}_{e}) to quantify the
17 influence of microstructure on the clay gross yielding. Gross is referred to distinguish, from the first yielding, that
18 followed by major plastic straining and occurring about the state boundary surface (Cotecchia and Chandler 2000).
19 S_{σ} has resulted to be ≥ 1 for unfissured sensitive clays. This finding implies that the natural microstructure may provide
20 the clay with a larger state boundary surface and larger strength with respect to the reconstituted. Fig. 8a shows,
21 instead, that for clays of whatever microstructure, but whose mesofabric includes fissuring, $S_{\sigma} < 1$ (Vitone and
22 Cotecchia 2011).
23
24
25
26
27
28
29
30
31
32
33
34
35
36
37
38
39
40
41

42 As implied by $S_{\sigma} < 1$, shear testing has shown that the state boundary surface, SBS, of the fissured clay is smaller
43 than that of the reconstituted clay, SBS*, irrespective of any other F-ID feature, as shown in Fig. 8b. Hence, for
44 fissured clays, even when the microstructure is strong with respect to that of the reconstituted, its influence on the clay
45 mechanics is overcome by fissuring. The latter makes the clay not only weaker than the corresponding unfissured clay,
46 but also weaker than the clay when reconstituted. Moreover, where for sensitive unfissured clays structure degradation
47 occurs with post gross yield compression and gives rise to a negative hardening component ($dS_{\sigma}/d\varepsilon_v^p < 0$ where ε_v^p is
48 the plastic volumetric strain), for fissured clays, structure strengthening post gross yield compression (Fig. 8b)
49
50
51
52
53
54
55
56
57
58
59
60
61
62
63
64
65

1 contributes to a positive hardening ($dS_{\sigma}/d\varepsilon_v^p > 0$).

2
3 In the following, the geotechnical characterisation of the fissured clays sampled at the sites indicated in Figs 1 and
4
5 2 will make reference to the framework in Fig. 8.

6
7
8 *The fissured clays within the slopes*
9

10 Table 1 reports the F-IDs of the clays sampled within the three aforementioned slopes (Figs 1 and 2; F-IDs also in
11 Fig. 7). With reference to the clays outcropping at PI hillslope, the data in the Table are referred separately to units
12 PD1 and PD2.
13
14

15
16 At all the sites of reference, there exist clays of fissuring intensity I6, whose mesofabric is characterised by fissures
17 splitting the clay into millimetre lens-shaped elements, called *scales* (AGI 1979). The mesofabric of the bentonite
18 clays from SCM, instead, is characterised by centimetre size clay elements, i.e. fissuring intensity I5, and for some of
19 the PI clays, fissuring intensity may be even lower, i.e. I5-I4. Also, the fissure orientation varies from single, F1, to
20 random, F3.
21
22

23 Table 1 reports also the ranges of the clay index properties and initial void ratios, e_0 , determined in the laboratory
24 according to ASTM standards. The clay fraction is highest for SCM clays. Almost all the samples can be classified as
25 CH, according to the USCS classification (Unified Soil Classification System; ASTM 1985) and are of medium (SCM
26 and SEN scaly clays) to high activity (BENT). Their consistency is high, except for BENT clay.
27
28

29 As resulting from x-ray diffraction analyses, the mineralogy of the medium activity SCM and SEN clays includes
30 large quantity of mixed-layer illite-smectite, along with some smectite. Pure smectite is dominant in BENT clay.
31
32

33 When reconstituted in the laboratory, the clays in Table 1 exhibit strength properties (defined as intrinsic by
34 Burland 1990) that are rather poor, due to their high plasticity. Hence, an intrinsic slope weakness stems from the
35 composition of the clays, which represents an internal predisposing factor of slope failure. However, since the strength
36 properties of natural clays depend not only on composition, but also on their natural structure (Burland 1990;
37 Cotecchia and Chandler 2000), the mechanical behaviour of the undisturbed fissured clay samples in Table 1 has been
38 also investigated. The applicability of the behavioural framework shown in Fig. 8 to the clays has then been verified.
39
40

41 The oedometer compression curves of the undisturbed clay samples are shown in Fig. 9, along with the relevant
42 ICLs. The curves confirm the framework in Fig. 8a, since for each natural fissured clay the compression curve is
43 located on the left of the ICL. Also, as typical for fissured clays, the curve has a mild curvature, with no abrupt drop in
44
45
46
47
48
49
50

1 stiffness at any pressure. This mild curvature is probably due to the combination of progressive packing of the clay
2 elements and the degradation of the intra-element bonding (Vitone and Cotecchia 2011). Fig. 10 shows variation in
3 specific volume, v , with the mean effective stress, p' , experienced by BENT clay specimens during isotropic
4 compression and undrained shear. The v - p' data confirm $S_o < 1$ for fissured clays also in isotropic compression.
5
6 Moreover, the contractive nature of the shear response of the specimens isotropically consolidated to v - p' states to the
7 left of the isotropic normal consolidation line of the reconstituted clay, INCL*, confirms that *wet* shear behaviour
8 (Schofield and Wroth 1968) and gross yielding occur on the left of INCL*. The undrained shear state paths of BENT
9 clay are shown in the q - p' plane in Fig. 11, where q is the deviator stress and both q and p' are normalised for v by
10 means of the equivalent pressure p_e^* on the INCL* (see Fig. 10). The data show that, according to Critical State Soil
11 Mechanics, *dry* behaviour is recorded only for specimens swelled to overconsolidation ratios $R (= p'_y/p')$ higher than
12 2, and that the q - p' states possible for the fissured clay are located inside the state boundary surface of the
13 reconstituted clay, SBS*. Thus, the data confirm the framework of shear behaviour in Fig. 8b, i.e. the size of the SBS
14 of the natural clay is smaller than that of the reconstituted, SBS*. The normalised stress paths of the fissured clay
15 specimens consolidated beyond gross yield before shearing, confirm that the *wet* side of the SBS of the fissured clay
16 (e.g., stress paths of specimens BENT-B and BENT-C in Fig. 11) increases in size with compression. Hence, a
17 positive hardening component adds to volumetric hardening for the fissured mesofabric.
18
19

20
21 All these behavioural features are common to all the clays in Table 1 (Vitone and Cotecchia 2011; Cotecchia et al.
22 2014). It is not possible to report all the test data for a matter of space, therefore the BENT shear data are meant as
23 representative of the behavioural trends exhibited by all the clays in the slopes of interest. These behavioural trends
24 allow to infer that each of the slopes of reference is weaker than it would be if it was formed of clays of the same
25 composition and consolidation state (i.e., having the same v - σ'_{ij} at all points, x - y - z , as those in situ; Fig. 12), but
26 reconstituted in the laboratory (Fig. 8). This is because for any clay element in the slope, of state v - σ'_{ij} (Fig. 12a),
27 fissuring causes a weakening with respect to the reconstituted clay, whatever the microstructure is like, as proven by
28 the smaller size of the SBS of the fissured clay with respect to that of the reconstituted, SBS*, in the q - p' - v space (Fig.
29 8b). The difference in size between the state boundary surfaces implies that, at any point in the slope (x - z : v - σ'_{ij} , Fig.
30 12a), the gross yield surface (yield surface in the figure) of the fissured clay is smaller than that of the reconstituted
31 clay, as exemplified respectively by YS_F and YS^* in Fig. 12b. Even stronger would be the slope if formed of the same
32 clay, but unfissured and sensitive, due to a microstructure stronger than that of the reconstituted clay.
33
34
35
36
37
38
39
40
41
42
43
44
45
46
47
48
49
50
51
52
53
54
55
56
57
58
59
60
61
62
63
64
65

1 Table 2 reports the peak friction angles measured for the natural fissured clays in Table 1, ϕ'_{peak} ($c'=0\text{kPa}$ is
2 assumed), the post-peak friction angles, $\phi'_{\text{post-peak}}$, and the critical state friction angles of the reconstituted, ϕ'_{cs} . These
3 values were deduced from consolidated undrained shear tests in the triaxial (CIU). The data suggest that fissuring not
4 only reduces the size of the SBS of the clay, but also the peak friction angles on the *dry* side (making them quite close
5 to ϕ'_{cs}), because it restrains the dilation rates of the overconsolidated clay. On the *wet* side, both the fissured clay and
6 the reconstituted clay friction angles are rather low. Given the void ratios (see Table 1) and gross yield pressures in the
7 slopes (Figs 9-10), the clays are overconsolidated in situ and exhibit a *dry* shear behaviour down to about 50-80 m,
8 beyond which they tend to show a *wet* shear behaviour. It follows that the clay strength parameters vary in a limited
9 range, despite their different origin, location and history, and provide the slopes with common weakness.

10 Table 2 also reports values of the residual friction angle, ϕ'_r , measured in the laboratory by means of either
11 Bromhead ring shear tests or reversal direct shear tests. These values are representative of the very low strength of
12 these high plasticity clays, in good agreement with those reported in the literature for clays of similar plasticity and
13 composition (Lupini et al. 1981; Stark and Hussain 2013).

14 Fig. 13 shows the saturated permeability values, k_s , measured in oedometer tests on the fissured clays in Table 1
15 and on the same materials when reconstituted. The measurements have been carried with consolidation flow in the
16 axial direction of the undisturbed sample. The k_s - e data refer to different stages of compression during the oedometer
17 test (Terzaghi 1923). The ratios $\Delta e/\Delta \log k_s$, generally defined as C_k (Taylor 1948), decrease with compression for both
18 natural and reconstituted clays, similarly to what has been observed by Terzaghi et al. (1996).

19 Fig. 13 also shows the k_s associated to the in situ void ratio (deduced from the linear regression of the test data and
20 indicated with circles). For the fissured samples, k_s results from the combination of both the very low permeability of
21 the clay elements between the fissures and the high permeability of the fissures (Federico and Musso 1990). The figure
22 shows that k_s of the fissured clay from laboratory testing is higher than 10^{-10} m/s and it is found to be higher (even of
23 two orders of magnitude) than that of the same clay when reconstituted.

24 For fissures oriented and orthogonal to the flux direction (as for SCM scaly clay, F1/0°), k_s is lower than that
25 measured for clays of random fissure orientation, (i.e., SEN scaly clay, F3), and further smaller (up to one order of
26 magnitude) than for those having fissures oriented in the direction of the flux (F1/90°). The larger permeabilities
27 resulting from fissuring predispose the slopes to larger rainfall infiltration. This makes possible an increase of the pore
28 water pressures down to large depths, which is detrimental for the field operational strengths. These effects will be

1 shown to apply to the slopes here of reference. Hence, it may be envisaged that fissuring plays the role of internal
2 factor predisposing the slope to failure not only for its effects on the clay mechanics, but also for its influence on the
3 clay permeability.
4

5 6 7 8 LANDSLIDE MECHANISMS IN SLOPES FORMED OF FISSURED CLAY SEQUENCES 9

10 *The Vadoncello landslide*

11 Fig. 3 reports the map and the lithological section of the Vadoncello slope (Santaloia et al. 2001; Fig. 2c). In the
12 section, the soils have been grouped into several soil complexes, according to a lithological screening and to the index
13 properties of the clay samples (Table 1). Each complex represents a lithological sequence found recurrent in the slope.
14
15

16 In December 1993, a medium depth rotational slipping took place at the top of the slope and was followed
17 downslope by an earth-flow (Hungr et al. 2014), characterised by both sliding along a shear band and full remoulding
18 within the landslide body. The earthflow deposit, identified as complex G in Fig. 3b (about 10 m deep), includes
19 remoulded scaly clays and rock debris. Landslide activity was monitored from 1994 until 1996 by means of both GPS
20 and inclinometers; also piezometric monitoring was on at the same time.
21
22
23
24
25
26
27

28 As said before, SEN clays are characterised by friction angles that are particularly low both at peak and post-peak
29 (Table 2). Furthermore, below 30-40 m depth they exhibit stress-strain states on the *wet* side (Santaloia et al. 2001),
30 with corresponding friction angle, ϕ' , lower than that of the dilative shallower clays. This condition, combined with
31 the small size of the SBS of the SEN clays, allows for the occurrence at depth of large plastic straining due to even
32 small changes in equilibrium (such as those effect of climate), and predisposes the slope to deep failure. Conversely,
33 clay fissuring at depth does not give rise to relatively high permeability values (Fig. 13) and, hence, it does not
34 predispose the slope to rainfall infiltration down to large depths. This has been confirmed by piezometers installed at
35 larger depths. They have shown the presence of a deeper groundwater system, location of rather permanent
36 piezometric heads; these are likely to be fed by the aquifer present in the karst limestone of the Picentini Mountains
37 (Fig. 4) and are not significantly affected by rainfalls (Santaloia et al. 2001). Only the piezometric levels monitored in
38 complex G have been found to be influenced by rainfall events in the short term (Santaloia et al. 2001).
39
40
41
42
43
44
45
46
47
48
49

50 In order to diagnose the failure mechanism and the triggering causes of the 1993 Vadoncello landslide, temporal
51 geomorphological analyses have been carried out. It has been found that the 1993 event had been preceded, in 1980,
52 by sliding in the lower part of the slope (Santaloia et al. 2001), subsidiary to the far larger and deeper Serra
53
54
55
56
57
58
59
60
61
62
63
64
65

1
2
3
4
5
6
7
8
9
10
11
12
13
14
15
16
17
18
19
20
21
22
23
24
25
26
27
28
29
30
31
32
33
34
35
36
37
38
39
40
41
42
43
44
45
46
47
48
49
50
51
52
53
54
55
56
57
58
59
60
61
62
63
64
65

dell'Acquara clay-slide, mobilised few hours after the 1980 Irpinia earthquake (V. Cotecchia et al. 1986). The Serra dell'Acquara landslide soils are named as complex I in Fig. 3b, at the toe of the Vadoncello slope, whereas the soils mobilised in the slope in 1980 represent complex H. Hence, the 1993 event was an evolution of a past instability. Furthermore, the analysis of the topographic monitoring data of 1995 (Fig. 14) shows that, while the highest displacement rates were taking place in the source area (area A in Fig. 14) and in the channel of the earth-flow (area B), the accumulation area (area C) was moving far more slowly, in a direction about parallel to the Serra dell'Acquara axis. GPS monitoring showed that this latter body was moving too, although very slowly, and II inclinometer monitoring (Fig. 3b), at the toe of the slope (area C, Fig. 14), gave evidence to the occurrence of sliding at 15 m depth within the Serra dell'Acquara clay slide. Therefore, the landslide reactivated in 1993 was the combination of a relatively fast shallow landslide process and a deeper, far slower deformation process, resulting from the interaction of the Vadoncello slope with the very slowly active Serra dell'Acquara clay-slide (Figs 3 and 14). The moving slope toe may be then recognized as the trigger of variations with time of the slope geometry. Given the available soil strengths, this brought the slope to instability in 1993, with rotational slipping at the top and earthflowing down-slope (Santaloia et al. 2001).

Numerical modelling was carried out by means of the finite difference code FLAC 2D (Itasca Consulting Group 2000), implementing the geotechnical model shown in Fig. 15, extended upslope of about 500 m (Santoro 1999; Cotecchia et al. 2000). Based on laboratory test results (Tables 1 and 2, Figs 8, 9 and 13), the geotechnical model includes the different soil complexes, all modelled using a linear elasto-plastic non associated Mohr-Coulomb model, with strain softening post-peak. Dilative and contractive zones (of *dry* and *wet* behaviour, respectively) were distinguished within each complex (Cotecchia et al. 2000), the *wet* portions being characterised by $c'=0$ kPa and $\phi'=\phi'_{cs}$ yield parameters, whereas for the dilative portions, c' and ϕ' values shown in Fig. 15 were used. Yield was assumed to be reached at about 10% shear strain and followed by strain softening, to a yield locus characterised by $c'=0$ kPa and $\phi'_r=5.5^\circ$ (reached at 50% shear strain). Both the shallow and the deep groundwater systems were modelled, considering the piezometric levels compatible with the two water tables in Fig. 15. A very slow-moving boundary at the slope toe was also implemented in the numerical model, in order to simulate the Serra dell'Acquara landsliding. The numerical results, in terms of displacement values, are synthesized in Fig. 16. Each boundary within areas 1, 2 and 3 is characterised by quasi-uniform displacements (average values in the figure). These represent the results of three numerical analyses: A) no seepage and pure submersion of the soils below the two different water

1 tables, B) seepage complying with the different water tables in the deep and shallow seepage domains, but no toe
2 translation, and C) both seepage and toe translation. The numerical results confirm that the internal slope factors and
3 the toe boundary condition combine to generate a complex landslide mechanism: a rather fast rotational slipping
4 upslope (area 1 in Fig. 16) and a shallow earthflow downslope. In particular, the earthflow is predicted to reach
5 inclinometer I1 only when the moving toe boundary is modelled. Furthermore, numerical modelling confirms the
6 occurrence of lower rate movements at larger depths.
7
8
9

10
11
12 The SEN case study exemplifies how, in the Apennines, often shallow fast landslides may be just the local
13 outcropping of far larger and deeper systems at marginal stability.
14
15
16
17

18 *The Pisciolio landslide basin*

19
20 Fig. 5 reports the geological setting of the PI hillslope (Fig. 2c), location of clayey turbidites of the Paola Doce
21 Formation (PD 1 and PD2 clays in Table 1). Due to the presence of an anticline, that caused uplifting of the central
22 portion of the hillslope, Red Flysch outcrops in the centre of the landslide basin (Fig. 5). Also, a normal fault crosses
23 the hillslope with an East-West trend and separates northern and southern sectors. In the past, this fault was location of
24 a deep gorge, hosting the Pisciolio stream (Fig. 5), whose section size progressively decreased in the last 50 years.
25
26
27
28
29

30 Clay fraction and plasticity index decrease moving from the lower PD1 clays to the upper PD2 (Table 1). The
31 compression behaviour, strength parameters and permeability values of these clays are shown in Fig. 9, Table 2 and
32 Fig. 13 respectively.
33
34
35

36 Ten clay-slides are located within the PI hillslope (Fig. 5). They are moving at rates from few millimetres to tens
37 of centimetres per year (Cotecchia et al. 2014), causing damage to both the Apulian Aqueduct pipeline and the road
38 located at the base of the slope. The most severe damage has been observed in the southern portion of the hillslope,
39 where landslides C9, C and A are located (Fig. 5). These landslide bodies, involving both PD and RF clays, have a
40 common toe about the road, intercepted by inclinometer I12 (Fig. 17). Inclinometer I5, installed in the central part of
41 body A, gives also evidence to the retrogression of movements upslope, down to large depths, although so far it has
42 not been sharply bent at any depth. In Fig. 17 the inclinometer data intercepting the shear bands of bodies L and G are
43 also reported (Fig. 5). Based on the data, the landslides at PI can be classified as multiple retrogressive landslides, of
44 medium to large depth (Fig. 5b).
45
46
47
48
49
50
51
52
53

54 The piezometric levels have been found to reach few metres below ground level in several piezometers (Fig. 5)
55
56
57
58
59
60
61
62
63
64
65

1 installed from small to large depths (i.e., 60 m). As discussed earlier, the laboratory measurements showed that the
2 saturated permeability of the PD clays can be even higher than 10^{-10} m/s at the element scale (Fig. 13). Moreover, k_s
3 higher than 10^{-9} m/s has been measured in situ, through constant head permeability tests (Pedone 2014). Such a
4 relatively high permeability of the clay matrix, together with the higher permeability of the rock strata, ease the
5 rainfall infiltration and the occurrence of high piezometric heads and low shear strengths down to large depths.
6
7

8
9
10 Limit equilibrium back-analyses (Morgenstern and Price 1965), implementing the measured piezometric heads,
11 have been performed to evaluate the operational friction angles. These have been found to be either close to the peak
12 friction angles, e.g. bodies A, C, G and L, or to the post-peak ones, e.g. bodies F and C9 (see Table 2). Therefore,
13 landslide bodies A, C, G and L represent first-time failure processes, whereas bodies F and C9 represent an evolution
14 of past failures, in agreement with the temporal analysis of aerial photos. In 1955 (Fig. 18), only bodies F and C9 were
15 present, although smaller than today; only soil slips occurred in the southern slope sector. At that time, the Pisciolò
16 stream flew in a deep gorge, representing the main discharge path of the water run off on the slope. Subsequent aerial
17 photos show that, in the last 60 years, progressive widening and deepening of landsliding have taken place. At the
18 same time, the section of the Pisciolò stream has decreased, with a consequent loss of discharge capacity. It is
19 envisaged that this has promoted rainwater ponding, infiltration and increase of the piezometric levels, bringing about
20 the widening and deepening of landsliding.
21
22
23
24
25
26
27
28
29
30
31

32 As shown in Fig. 19, with particular reference to the toe of bodies C9, C and A, a seasonal variation characterises
33 the current landslide displacement rates, both at depth (inclinometer I12) and at ground surface (GPS sensor S2), with
34 maximum values at the end of winter and minimum values at the end of summer. Also the piezometric heads
35 measured in the same area (cells at 15 and 36 m depth along P7) and the 180-day cumulated rainfall (recorded at the
36 Melfi weather station) follow a similar fluctuation trend. Hence, the pluviometric regime of the area and the clay
37 hydraulic properties appear to allow for seasonal variations of the pore pressures. These may trigger accelerations of
38 the fully developed landslide bodies, such as those measured at the toe of the slope in the southern sector (bodies C9
39 and C; Fig. 5). Piezometric data similar to those shown in Fig. 19 have been collected all over the hillslope.
40
41
42
43
44
45
46
47
48

49 The transient seepage in the slope, influenced by the slope-atmosphere interaction, has been modelled by means of
50 finite element analyses of a two-dimensional slope model, implementing the hydraulic permeabilities and the water
51 retention properties measured both in situ and in the laboratory (Cotecchia et al. 2014; Pedone 2014). In particular, the
52 FEM code Seep/w (GeoSlope International Ltd. 2004), that integrates the Richards' equation (1931), has been used to
53
54
55
56
57
58
59
60
61
62
63
64
65

1 model the slope section II in Fig. 5b. The mesh of the model shown in Fig. 20 is formed of quadrilateral elements. The
2 saturated permeability of both PD1 and PD2 clays has been set as $k_s=1*10^{-9}$ m/s, according to the above mentioned in
3
4 situ measurements. Only for the top layers that happen to be above the water table during part of the year, the model
5
6 accounts for the water retention curve measured in the laboratory on samples taken by 2 m depth (Cotecchia et al.
7
8 2014). Retention data have been fitted using the van Genuchten (1980) equation, while the hydraulic conductivity
9
10 model proposed by the same author has been employed to simulate the variation of the permeability coefficient with
11
12 suction. Furthermore, an organic top soil layer has been implemented, whose saturated permeability is $k_s=1*10^{-8}$ m/s.
13
14 Pore pressures constantly equal to zero have been imposed at the very top and at the bottom of the slope, according to
15
16 the presence of a spring and of the Ofanto River respectively. The lowest boundary of the model has been assumed as
17
18 impermeable, whereas the net rainfalls referred to the period September 2006-August 2007 have been cyclically
19
20 applied at the top of the mesh. Net rainfalls result from the difference between total rainfalls and evapo-transpiration
21
22 fluxes, the latter evaluated by means of the FAO Penman-Monteith method (Allen et al. 1998).
23

24 The numerical results have been compared with the piezometric data logged down the verticals P7 and P5 (Figs 5b
25
26 and 20) for modelling validation (Fig. 21). The variations in piezometric head predicted by the numerical model
27
28 (continuous lines in Fig. 21) are close to those measured (squares in Fig. 21) down borehole P7, especially once the
29
30 fractured rock inclusions are also implemented in the analyses ($k_s = 10^{-6}$ m/s). On the contrary, the predicted
31
32 fluctuations are much smaller than those recorded along the vertical P5 (Fig. 21). This vertical is very close to the
33
34 sandy deposit N (Fig. 5a) and this is probably causing three-dimensional effects not accounted for in the 2D numerical
35
36 modelling.
37

38 The Pisciola case study is representative for landsliding influenced by the slope-atmosphere interaction recurrent
39
40 in the Southern Apennines. In particular, at Pisciola, this interaction is a triggering cause that combines with the
41
42 internal predisposing factors cited before.
43
44
45

46 *The Santa Croce di Magliano landslides*

47 As depicted in Fig. 6, the slopes at SCM are formed by turbidites part of the Daunia Unit (Fig. 2c) and are diffusely
48
49 location of failure processes. These start in the scaly clay strata (SCM scaly clay soils), whose mesofabric and
50
51 geotechnical properties have been discussed above (Figs 9-11 and 13, Tables 1 and 2). Thereafter they involve the
52
53 BENT clays and the FAE rock slab (Fig. 6) located upslope. Most of the sliding surfaces have toe about the river
54
55
56
57
58
59
60
61
62
63
64
65

1 flowing at the bottom of the valleys, either North or South of the village (Fig. 6). Several springs occur about the rock-
2 clay contact, which represent the outcropping of a seepage domain whose water table occurs at 2-3 m depth below the
3 slope ground surface.
4

5
6 The SCM scaly clays, along with the BENT clays, are of even higher plasticity than the SEN and PI clays (Fig. 2;
7 Table 1). Due to these intrinsically weak clays, fissuring provides a further source of strength reduction. Moreover, in
8 this case, the clay strength does not benefit from the presence of as many coarse strata and floating rock beddings as
9 for the SEN and the PI slopes. Within the simpler SCM sequences (Fig. 6b), the landslide mechanisms are mainly
10 roto-translational sliding, as shown by the inclinometer data in Fig. 6c. This intercepted a sliding surface at 22 m
11 depth, along which the displacement rates were about 14 mm/month during a period of high landslide activity (Fig.
12 6c).
13
14
15
16
17
18
19

20 The failure mechanism recognized in the southern slope location of the inclinometer may be considered
21 representative for most of the sliding phenomena at SCM (Cotecchia et al. 2007; Fig. 6a). The only difference between
22 the northern and the southern slopes of SCM promontory is that, where in the northern slopes landsliding has been on
23 for a longer period, reaching and involving the top FAE rock slab (Fig. 6), in the southern slopes, it is more recent and
24 caused more limited variations of the original morphologies. The back-analyses of the northern landslides result in
25 mobilised friction angles $\phi'_m = 17^\circ - 18^\circ$ ($c' = 0$ kPa), which are far above the residual friction angle of the clays (Table
26 2) and only a bit lower than the clay peak friction angles on the *dry* side (Cotecchia et al. 2003, 2007). Conversely, the
27 mobilised friction angles for the southern landslides are smaller, $\phi'_m = 12^\circ - 13^\circ$. The high operational strengths in the
28 northern slopes may appear in contrast with the more mature activity of landsliding in such slopes. However, it should
29 be considered that the long-term landsliding in these slopes has caused remoulding of the scaly clays that brings about
30 an increase in the shear strength of the clays, as shown by the framework in Fig. 8b. This remoulding has not taken
31 place yet in the southern slopes of the promontory, which, therefore, are weaker than at North.
32
33
34
35
36
37
38
39
40
41
42
43
44
45
46

47 CONCLUSIONS

48 The three case studies have given evidence to the failure processes that may take place and bring about landsliding in
49 slopes formed of tectonized turbidites. The landslide mechanism may be either simple non-circular sliding (SCM), or
50 multiple retrogressive clay sliding (PI), or a combination of deep sliding with shallow earth-flowing (SEN) but, in
51 general, it is of medium depth to deep and slow to extremely slow.
52
53
54
55
56
57
58
59
60
61
62
63
64
65

1 The tectonized soil sequences belong to different geological formations, but share major similarities in the hydro-
2 mechanical behaviour of the clays, which are the weakest lithotype within the slopes and control the failure
3 progression. These mechanical properties have been shown to fit a framework where the fissured clay strength is not
4 only lower than that of the unfissured structured clay, but also than that of the unfissured reconstituted clay. This
5 finding has allowed to recognise, as first, that slopes in fissured clays are weaker than slopes in reconstituted clays; as
6 second, that the mechanical properties of the high plasticity fissured clays are an internal predisposing factor of
7 landsliding.
8
9

10 The clay fissuring and the fractured rock interbeddings have also been recognized as sources of larger field
11 permeabilities, which predispose the slopes to infiltration rates down to large depths higher than those expected for
12 clays. This hydraulic feature allows for large piezometric heads at depth and relatively smaller available strengths.
13 Failure has been found to start generally in the fissured clays and to propagate depending on the slope stratigraphic
14 features. These, along with both the mechanical and hydraulic boundary conditions of the slope system, control the
15 type of landslide mechanism. For example, simple sliding is more likely to occur in slopes of simpler stratigraphy and
16 characterised by standard boundary conditions, such as the SCM slopes. Here, three main soil strata, slightly dipping
17 downslope, occur from bottom to top. More complex sliding, or otherwise earth-flowing, is more likely to occur in
18 slopes of more complex stratigraphy, where the soil sequences are more chaotic, as at PI and SEN. Furthermore, earth-
19 flowing at SEN has been recognized to be only the shallow process within a wider and deeper failure mechanism,
20 which relates to a moving boundary at the slope toe. Such landslide features have been verified by numerical
21 modelling and also found to apply at other sites in the southern Apennines, e.g. Toppo landslide (Cotecchia et al.
22 2009).
23
24

25 Finally, it has been shown that slide accelerations recorded at the end of winter–early spring may be due to the
26 reach of maximum pore water pressures as effect of cumulated seasonal rainfall infiltration. The seasonal piezometric
27 excursions have been measured and, thereafter, predicted through a rather accurate modelling of the transient seepage
28 in the slope, accounting for the hydraulic soil properties, both when saturated and in partial saturation conditions.
29
30
31
32
33
34
35
36
37
38
39

40
41
42
43
44
45
46
47
48
49
50
51 *Acknowledgments*

52 The authors wish to thank the Apulian Aqueduct SPA (2008-2011), the Apulia Region (PS_119- 2006-2010), the
53 Italian Ministry for Research and University (PRIN 2001, 2007, 2010-2011) and European Community-Environment
54 Programme (1994-1996) for providing the financial support that has permitted the studies discussed in the paper.
55
56
57
58
59
60
61
62
63
64
65

REFERENCES

- 1 AGI (1979) Some Italian experiences on the mechanical characterisation of structurally complex clay soils. In
2 International Society of Rock Mechanics (ed.), Int Soc Rock Mech 4th Int Cong 1, pp 827-846
- 3 Airò Farulla C, Ferrari A, Romero E (2010) Volume change behaviour of a compacted scaly clay during cyclic suction
4 changes. *Canadian Geotechnical Journal* 47(6):688-703
- 5 Allen RG, Pereira LS, Raes D, Smith M (1998) Crop evapo-transpiration, guidelines for computing crop water
6 requirements. FAO irrigation and drainage paper 56
- 7 ASTM (1985) Classification of Soils for Engineering Purposes: Annual Book of ASTM Standards, D 2487-83, 04.08,
8 American Society for Testing and Materials, pp 395-408
- 9 BSI British Standards (1986) Code of practice for foundations. BSI BS8004
- 10 Burland JB (1990) On the compressibility and the shear strength of natural clays. *Géotechnique* 40(3):329-378
- 11 Calabresi G, Manfredini G (1973) Shear strength characteristics of the jointed clay of S. Barbara. *Géotechnique*
12 23(2):233-244
- 13 Cicolella A, Picarelli L (1990) Decadimento meccanico di una tipica argilla a scaglie di elevata plasticità. *Italian*
14 *Geotechnical Journal* 24:5-23
- 15 Cotecchia F, Chandler RJ (2000) A general framework for the mechanical behaviour of clays. *Géotechnique*
16 50(4):431-447
- 17 Cotecchia F, Santaloia F (2003) Compression behaviour of structurally complex marine clays. *Soft Ground*
18 *Engineering in Coastal Areas; Proc Nakase Memorial Symp, Yokosuka Japan*, pp 63-72
- 19 Cotecchia F, Vitone C (2011) On the model requirements to predict the behaviour of fissured clays. XV ECSMGE,
20 Athens, Greece, pp 525-530
- 21 Cotecchia F, Santaloia F, Santoro F (2000) Movements in a tectonized soil slope: comparison of monitoring data and
22 modelling results. *Int Conf Geotechnical & Geological Engineering, Melbourne, Australia*
- 23 Cotecchia F, Cafaro F, Melidoro G, Mitaritonna G (2003) Mechanical behaviour of natural tectonized bentonites. *Proc*
24 *Int Workshop Geotechnics of Soft Soils, Amsterdam*, pp 397-402
- 25 Cotecchia F, Vitone C, Cafaro F, Santaloia F (2007) The mechanical behaviour of intensely fissured high plasticity
26 clays from Daunia. *Proc 2nd Int Workshop Characterisation and Engineering Properties on Natural Soils,*
27 *Singapore, Taylor & Francis London*, pp 1975-2003
- 28 Cotecchia F, Mitaritonna G, Elia G, Santaloia F, Lollino P (2009) Meccanismi di frane in pendii in argille dell'Italia
29 Meridionale ed effetti delle precipitazioni meteoriche. *1st Int Workshop on Landslides: rainfall induced landslide*
30 *and nowcasting models for early warning system*, pp 31-43
- 31 Cotecchia F, Santaloia F, Vitone C, Palladino G (2012) A slow and complex landslide process in the Southern
32 Apennines (Italy). *Proceedings 11th Int Symp Landslides and 2nd North American Symp Landslides. Banff,*
33 *Alberta, Canada, in Landslides and Engineered Slopes: Protecting Society through Improved Understanding,*
34 *Taylor & Francis Group 1*, pp 1009-1016
- 35 Cotecchia F, Pedone G, Bottiglieri O, Santaloia F, Vitone C (2014) Slope – atmosphere interaction in a tectonized
36 clayey slope: a case study. *Italian Geotechnical Journal* 1:34-61
- 37 Cotecchia V (1986) Ground displacement and slope instability triggered off by the earthquake of November 23, 1980
38 in Campania and Basilicata. *Int Symp Engineering geology problems in seismic areas, Geol App Idr* 21:31-100
- 39 Croce A (1971) Opening address of the International Symposium on 'The Geotechnics of structurally complex
40 formations'. *Capri 2*, pp 148-151
- 41 Cruden DM, Varnes DJ (1996) Landslides types and processes. In: Turner AK, Schuster RL (eds) *Landslides:*
42 *investigation and mitigation, Transp Research Board Special Report 247. National Academy Press, WA*, pp 36-75
- 43 Dewey JF, Helman ML, Turco E, Hutton DHW and Knott SD (1989) Kinematics of the Western Mediterranean. In
44 *MPD Coward, D Park, RG (Editor), Alpine Tectonics. Geological Society*, pp 265-283
- 45 Di Nocera S, Matano F, Pescatore T, Pinto F, Quarantiello R, Senatore M R, Torre M (2006) Schema geologico del
46 transetto Monti Picentini orientali - Monti della Daunia meridionali: unità stratigrafiche ed evoluzione tettonica del
47 settore esterno dell'Appennino meridionale. *Boll Soc Geol It* 125:1-20
- 48 Desrues J, Viggiani G (2004) Strain localization in sand: an overview of the experimental results obtained in Grenoble
49 using stereophotogrammetry. *Int J Numer Anal Meth Geomech* 28:279-321
- 50 Doglioni C (1991) A proposal of kinematic modelling for W-dipping subduction – Possible applications to the
51 Tyrrhenian Apennines system. *Terra Nova* 3:423-434
- 52 EC Project Report (1996) *Landslide evolution controlled by climatic factors in a seismic area. Prediction methods and*
53 *warning criteria. Final Technical Report*
- 54 Fearon R, Coop M R (2000) Reconstitution - what makes an appropriate reference material? *Géotechnique* 50(4):471-
55 477
- 56
57
58
59
60
61
62
63
64
65

- 1 Fearon R, Coop MR (2002) The influence of landsliding on the behaviour of a structurally complex clay, *Quarterly*
2 *Journal of Engineering Geology and Hydrogeology* 35:25-32
- 3 Federico F, Musso A (1990) Consolidazione monodimensionale di argille a scaglie. Gruppo Nazionale di
4 coordinamento per gli studi di Ingegneria Geotecnica, Roma, pp127-130
- 5 Fenelli, GB, Paparo Filomarino M, Picarelli L, Rippa F (1982) Proprietà fisiche e meccaniche di argille varicolori
6 dell'Irpinia. *Rivista Italiana di Geotecnica* 3:110-124
- 7 Fookes PG, Denness B (1969) Observational studies on fissure patterns in cretaceous sediments of South-East
8 England. *Géotechnique* 19(4):453-477
- 9 Gasparre A, Nishimura S, Coop MR, Jardine RJ (2007) The influence of structure on the behaviour of London Clay.
10 *Géotechnique* 57(1):19–31
- 11 GEO-SLOPE International Ltd (2004) Seepage modeling with SEEP/W, user's guide. Calgary, Alberta, Canada
- 12 Hight DW, Gasparre A, Nishimura S, Minh NA, Jardine RJ, Coop MR (2007) Characteristics of the London Clay
13 from the Terminal 5 site at Heathrow Airport. *Géotechnique* 57(1):3-18
- 14 Hungr O., Leroueil S., Picarelli L. (2014) The Varnes classification of landslide types, an update. *Landslides* 11: 167-
15 194.
- 16 ISRM (1993) Metodologie per la descrizione quantitativa delle discontinuità nelle masse rocciose. *Italian*
17 *Geotechnical Journal* 2:151-197
- 18 Itasca Consulting Group (2000) FLAC2D Version 4.0. Minneapolis: Itasca Consulting Group
- 19 Leroueil S, Vaughan P (1990) The general and congruent effect of structure in natural soils and weak rocks.
20 *Géotechnique* 40(3):467-488
- 21 Lo KY (1970) The operational strength of fissured clays. *Géotechnique* 20(1):57-74
- 22 Lupini JF, Skinner AE and Vaughan PR (1981) The drained residual strength of cohesive soils. *Géotechnique*
23 31(2):181-213
- 24 Malinverno A, Ryan WBF (1986) Extension in the Tyrrhenian Sea and shortening in the Apennines as result of arc
25 migration driven by sinking of the lithosphere. *Tectonics* 5:227–245
- 26 Marsland A (1971) The shear strength of stiff fissured clays. *Roscoe Memorial Symp, Cambridge Univ*, pp 59-68
- 27 Melidoro A, Melidoro G, Panaro V (2002) Deformazioni gravitative dei versanti nei terreni fliscoidi con argille a
28 bentoniti di Santa Croce di Magliano (Molise). *Quarry & Construction*:11-17
- 29 Morgenstern NR, Price VE (1965) The analysis of the stability of general slip surface. *Géotechnique* 15(1):79-93
- 30 Morgenstern NR, Eigenbrod KD (1974) Classification of argillaceous soils and rocks. *Jour Geotech Eng Div, ASCE*
31 100(10):1137-1156
- 32 Ogniben L (1969) Schema introduttivo alla geologia del confine calabro-lucano. *Mem Soc Geol Ital*, 8:453-763
- 33 Parotto M, Praturlon A (2004) The Southern Apennine Arc. In U. Crescenti, S. D'Offizi, S. Merlino & L. Sacchi (eds),
34 *Geology of Italy, Special Volume of Italian Geological Society for the International Geological Congress* 32:33-58
- 35 Patacca E, Scandone P (2007) Geological interpretation of the CROP-04 seismic line (Southern Apennines, Italy). In:
36 Mazzotti A, Patacca E, Scandone P(Eds), *Results of the CROP Project, Sub-project CROP-04 So 7*, pp 297-315
- 37 Pellegrino A, Picarelli L (1982) Contributo alla caratterizzazione geotecnica di formazioni argillose intensamente
38 tettonizzate. *Geologia Applicata ed Idrogeologia* 20(2):155-192
- 39 Pedone G (2014) Interpretation of slow and deep landslides triggered by slope-atmosphere interaction in slopes
40 formed of fissured clayey turbidites. PhD thesis, Technical University of Bari, Italy
- 41 Pescatore T, Senatore MR (1986) A comparison between a present-day (Taranto Gulf) and a Miocene (Irpinian Basin)
42 foredeep of the Southern Apennines (Italy). *Spec Publs Int Ass Sediment* 8:169-182
- 43 Pescatore T, Renda P, Schiattarella M, Tramutoli M (1999). Stratigraphic and structural relationships between Meso-
44 Cenozoic Lagonegro basin and coeval carbonate platforms in southern Apennines, Italy. *Tectonophysics*315:269-
45 286
- 46 Pescatore T, Di Nocera S, Matano F, Pinto F (2000) L'Unità del Fortore nel quadro della geologia orientale dei Monti
47 del Sannio (Appennino Meridionale). *Boll Soc Geol It* 119:587–601
- 48 Petley DJ (1984) Shear Strength of Over-Consolidated Fissured Clay. *Landslides; Proc Int Symp 2*, pp 167-172
- 49 Picarelli L, Olivares L (2004) Mechanical behaviour of highly sheared clay shales. *Advances in Geotechnical*
50 *Engineering: The Skempton Conference - Advances in Geotechnical Engineering, ICEL*, pp 580-591
- 51 Richards LA (1931) Capillary conduction of liquids through porous media. *Physics* 1:318-333
- 52 Santaloia F, Cotecchia F, Polemio M (2001) Mechanics of a tectonized soil slope: influence of boundary conditions
53 and rainfalls. *Quart Journ of Eng Geol* 34:165-185
- 54 Santoro F (1999) Meccanismi di deformazione di pendii in formazioni strutturalmente complesse. Il caso della frana
55 Serra dell'Acquara – Vadoncello (Senerchia – AV). PhD thesis, Technical University of Bari, Italy
- 56 Scrocca D, Carminati E, Doglioni C (2005) Deep structure of the southern Apennines, Italy: Thin-skinned or thick-
57
58
59
60
61
62
63
64
65

skinned? *Tectonics* 24:1–20.

- 1 Schofield AN, Wroth CP (1968) *Critical state soil mechanics*. London: McGraw-Hill
- 2 Sella N, Dorci C, Riva A (1988) Sintesi geopetrolifera della Fossa Bradanica (avanfossa della catena appenninica
- 3 meridionale). *Mem Soc Geol It* 41:87–107
- 4 Silvestri F, Vitone C, d’Onofrio A, Cotecchia F, Puglia R, Santucci de Magistris F (2007) The influence of meso-
- 5 structure on the mechanical behaviour of a marly clay from low to high strains. *Geotechnical Tatsuoka*
- 6 *Symposium*, Rome, Hoe I Ling et al eds, *Soil Stress-Strain Behaviour: Measurement, Modelling, Analysis*,
- 7 Springer, the Netherlands, pp 333-350
- 8 Stark T, Hussain M (2013) Empirical Correlations: Drained Shear Strength for Slope Stability Analyses. *J Geotech*
- 9 *Geoenviron Eng*, 139(6): 853–862
- 10 Taylor DW (1948) *Fundamentals of soil mechanics*. John Wiley & Sons, New York
- 11 Terzaghi K (1923) Die Berechnung der Durchlässigkeit des Tones aus dem Verlauf der hydrodynamischen
- 12 Spannungserscheinungen. *Sitzungber. Akad Wiss Wien* 132, pp 125-138
- 13 Terzaghi K (1936) Stability of slopes in natural clays. *Proc. 1st Conf. On Soil Mechanics*, Harvard, 1: 161-185
- 14 Terzaghi K (1950) Mechanisms of landslides. *Geological Society of America*, Berkley, pp 83-123
- 15 Terzaghi K, Peck RB, Mesri G (1996) *Soil mechanics in engineering practice*. John Wiley & Sons, New York
- 16 van Genuchten MT (1980) A closed form equation for predicting the hydraulic conductivity of unsaturated soils. *Soil*
- 17 *Science Society of America Journal*, 44:892-898
- 18 Vitone C (2005) *Comportamento meccanico delle argille da intensamente a mediamente fessurate*. PhD thesis,
- 19 Technical University of Bari, Italy
- 20 Vitone C, Cotecchia F (2011) The influence of intense fissuring on the mechanical behaviour of clays. *Geotechnique*
- 21 61(12):1003-1018
- 22 Vitone C, Cotecchia F, Desrues J, Viggiani G (2009) An approach to the interpretation of the mechanical behaviour of
- 23 intensely fissured clays, *Soils & Foundation Journal* 49(3):355-368
- 24 Vitone C, Cotecchia F, Viggiani G (2012) Localisation processes and size effects for fissured clay specimens.
- 25 *Advanced Multiphysical Testing of Soils and Shales (AMTSS) Workshop In Springer Series in Geomechanics and*
- 26 *Geoengineering*, Laloui Ferrari Eds, pp 219-225
- 27 Vitone C, Cotecchia F, Viggiani G, Hall SA (2013a) Strain fields and mechanical response of a highly fissured
- 28 bentonite clay, *Int J Numer Anal Meth Geomech* 37:1510-1534
- 29 Vitone C, Viggiani G, Cotecchia F, Hall SA (2013b) Localized deformation in intensely fissured clays studied by 2D
- 30 digital image correlation, *Acta Geotechnica* 8:247-263
- 31 Walker BF, Blong RJ, McGregor JP (1987) *Landslide classification, geomorphology and site investigation*. *Soil Slope*
- 32 *Instability and Stabilisation The Netherlands: Balkema*, pp 1-5
- 33
- 34
- 35
- 36
- 37
- 38
- 39
- 40
- 41
- 42
- 43
- 44
- 45
- 46
- 47
- 48
- 49
- 50
- 51
- 52
- 53
- 54
- 55
- 56
- 57
- 58
- 59
- 60
- 61
- 62
- 63
- 64
- 65

1
2
3
4
5
6
7
8
9
10
11
12
13
14
15
16
17
18
19
20
21
22
23
24
25
26
27
28
29
30
31
32
33
34
35
36
37
38
39
40
41
42
43
44
45
46
47
48
49
50
51
52
53
54
55
56
57
58
59
60
61
62
63
64
65

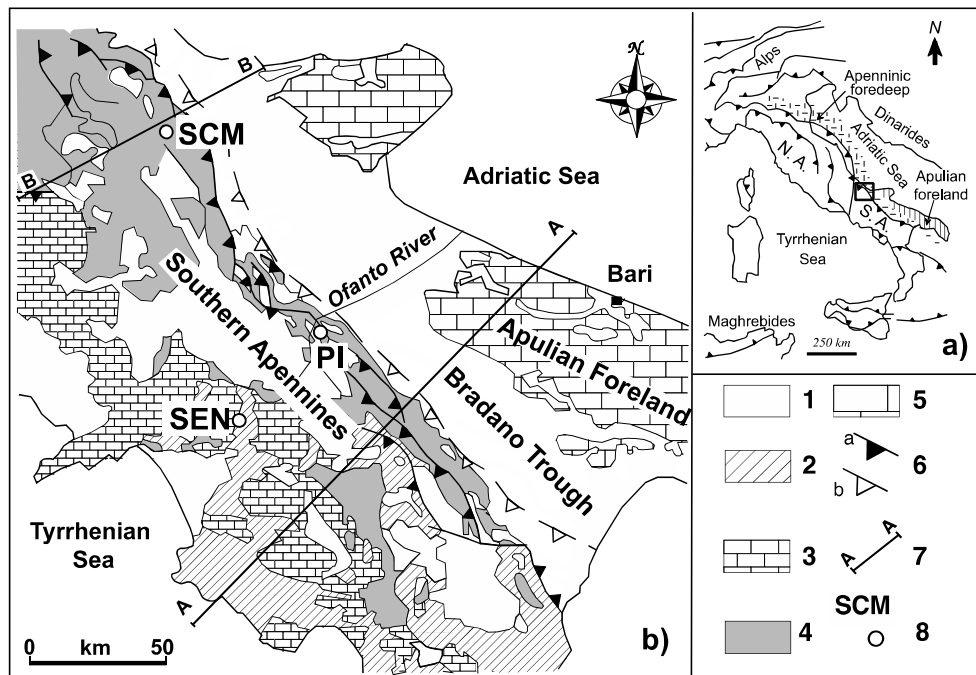


Fig. 1 (a) Schematic structural map of Italy (N.A. - Northern Apennines, S.A. - Southern Apennines) and (b) simplified geological map of the Southern Apennines (modified from Scrocca et al. 2005). Key: (1) marine to continental deposits, thrust-sheet-top deposits (Late Pliocene-Holocene); (2) Liguride-Sicilide Units and related ancient thrust-sheet-top deposits; (3) Apennine Platform Units and related silicoclastic foredeep deposits; (4) Lagonegro-Molise Units and related silicoclastic foredeep deposits; (5) Apulian Platform Units; (6) main thrusts (a) and buried Apenninic thrust front (b); (7) cross-section lines shown in Fig 2c; (8) slopes discussed in the paper (SEN-Vadoncello slope; PI-Pisciolo hillslope; SCM – Santa Croce di Magliano slopes).

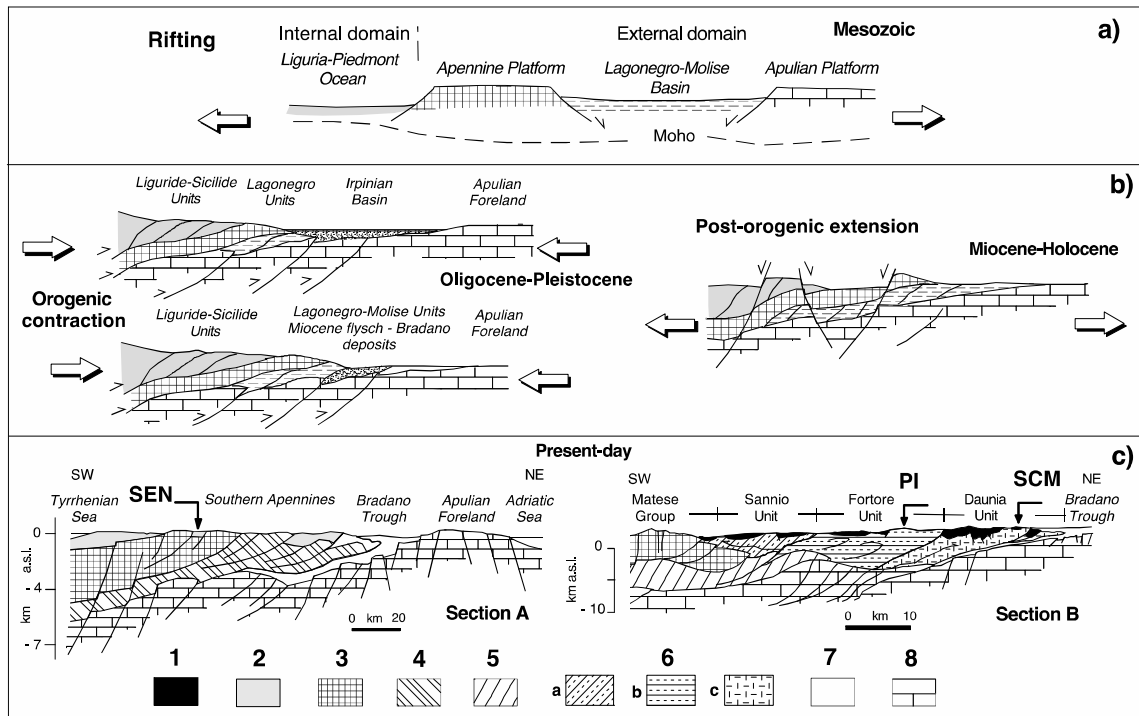


Fig. 2 Paleogeographic domains of the Southern Apennines during the Mesozoic Era (a), geological sketches (b) showing the main tectonic events responsible for the emplacement of the Southern Apennines (not to scale; after Parotto and Praturlon 2004, modified); c) schematic geological cross sections through both the southern Apennines thrust belt-foredeep-foreland system (Section A; after Sella et al. 1988, modified) and the north-eastern edge of the Sannio-Daunia Apennines (Section B; after Pescatore et al. 2000) - location of the sections in Fig. 1. Key: (1) plio-miocenic silicoclastic units; (2) Liguride-Sicilide Units (SEN soils); (3) Apennine Platform Units; (4) undifferentiated Lagonegrese-Molise Units; (5) lower sequences of the Lagonegrese-Molise Units; (6) upper sequences of the Lagonegrese-Molise Units (a: Sannio Unit, b: Fortore Unit – PI soils, c: Daunia Unit – SCM soils); (7) Bradano Trough Unit; (8) Apulian Platform Units.

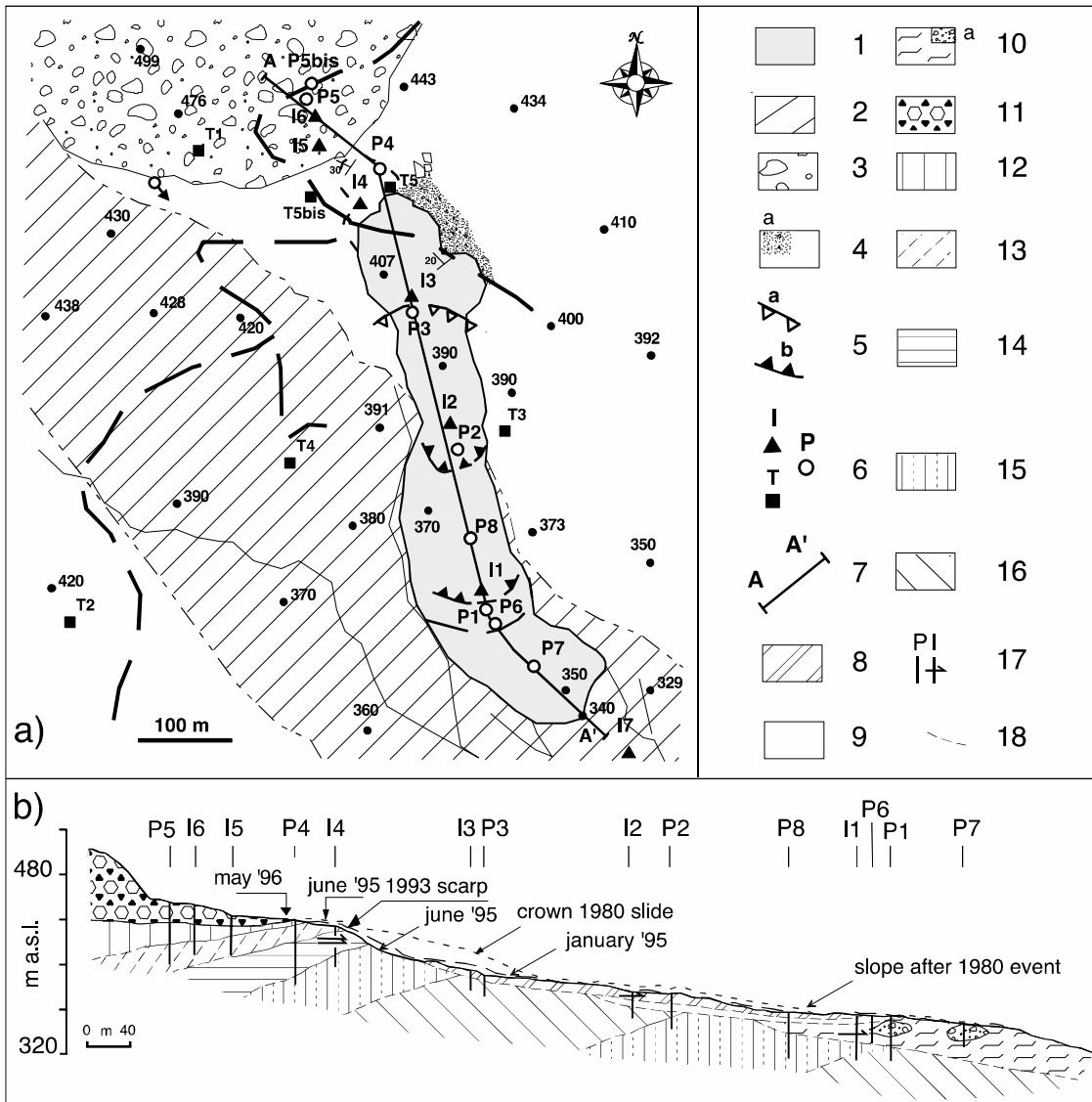


Fig. 3 Geological map (a) and section A-A' (b) of the Vadoncello slope (after EEC project 1996, Santaloia et al. 2001, modified); Keys: 1) 1993-'95 Vadoncello landslide; 2) Serra dell'Acquara landslide; 3) debris slab; 4) Variegated Clay Formation (SEN soils) with calcareous detritus (a); 5) 1980 crown (a), internal toes (b); 6) P-piezometers, I-inclinometers and T-topographic control stations (after EEC Report 1996; modified); 7) line of the section A-A'; Soil Complexes: 8) G, 9) H, 10) I with calcareous blocks floating in it (a), 11) A, 12) B, 13) C, 14) D, 15) E, 16) F; 17) piezometers (P1-P8) and inclinometers (I1-I7) with depth of shearing; 18) sliding surface.

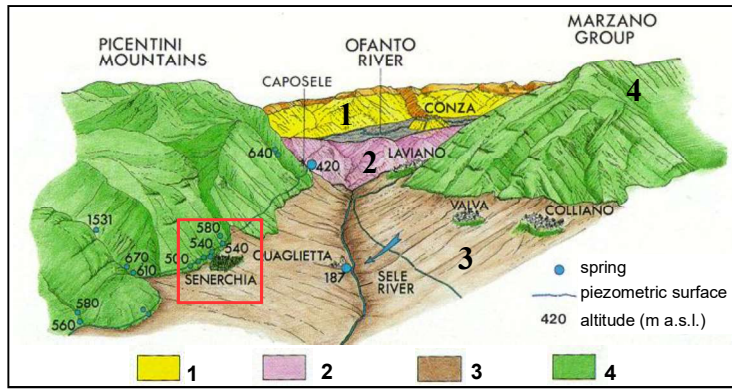


Fig. 4 Schematic view of the high Sele River Valley, location of the Senerchia slopes (after Cotecchia V. 1986, modified); Key: (1) Pliocene deposits; (2) Neogene and Sicilide Units; (3) Sicilide Unit (Lower Miocene-Cretaceous); (4) Apennine Carbonate Platform Units (Eocene-Upper Triassic).

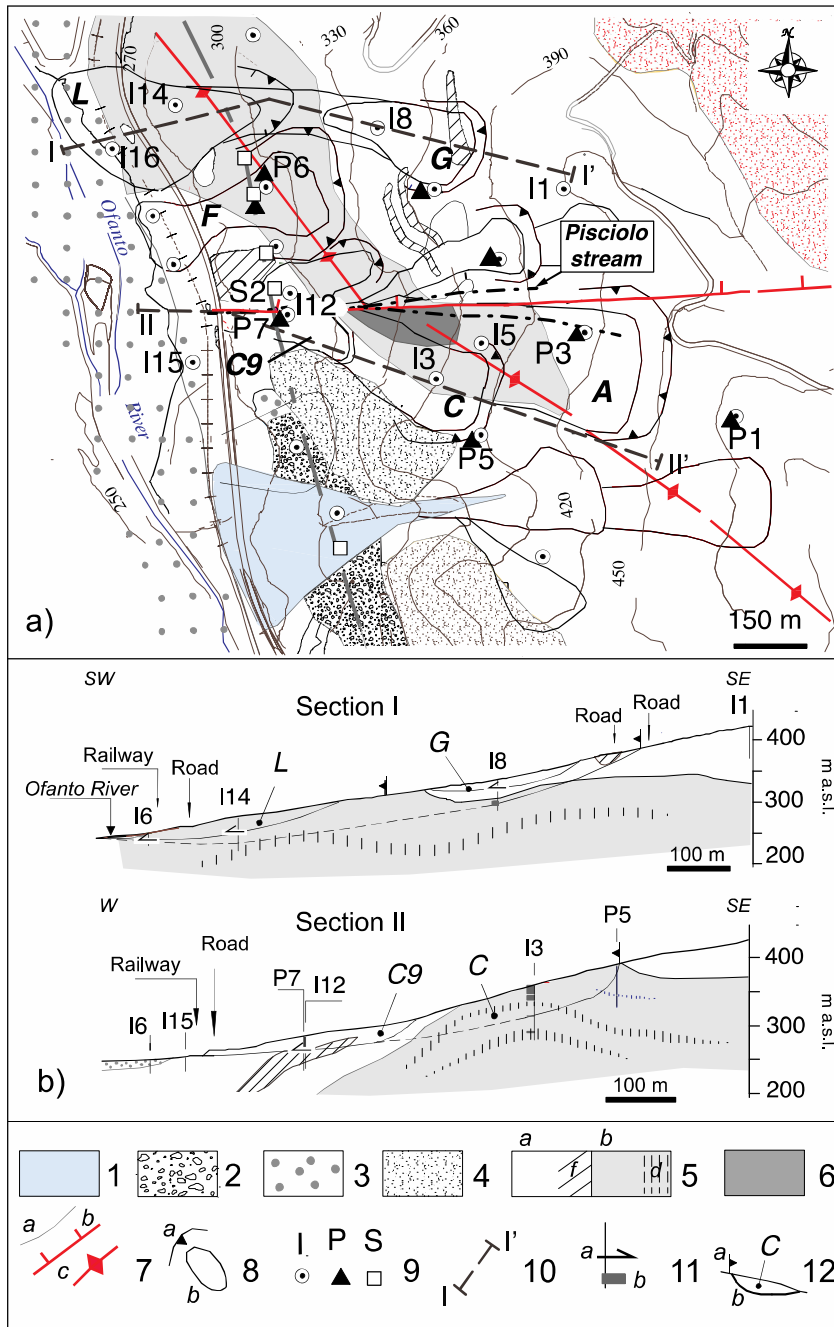


Fig. 5 Geological map (a) and sections (b) of Pisciole hillslope. Key: 1) fan deposit; 2) debris deposit; 3) alluvial deposit; 4) N; 5) PD2 (a) PD1 (b), f-locally fractured rocky strata, d-disarranged rocky strata; 6) R with rock or coarse-grained intervals; 7) stratigraphic contact (a), fault (b), anticline axis (c); 8) landslide: crown (a), body (b); 9) boreholes equipped with piezometers (P) or inclinometers (I), GPS sensor (S) – only the labels of the boreholes mentioned in this paper are reported; 10) line of the section shown in the frame b) of the figure; 11) boreholes: inclinometer shear bending (a), remoulded soil portions (b); 12) landslide: crown intercept (a), failure surface (b), dashed line when it is inferred.

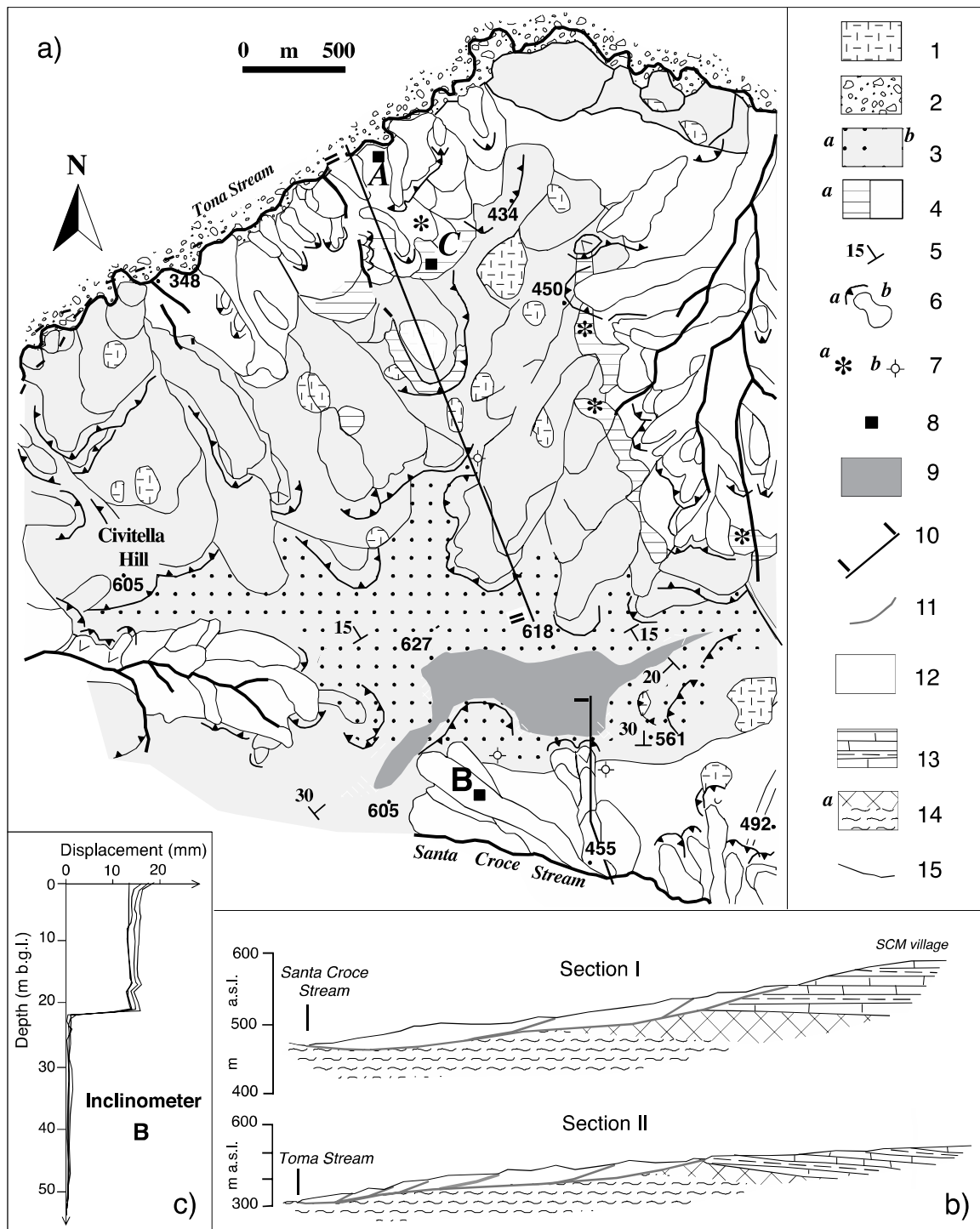






Fig. 6 Geological map (a) and sections (b) of Santa Croce di Magliano hill (after Melidoro et al. 2002), c) displacements, measured at depth within inclinometer B, after 1, 7, 8 and 9 months since the zero reading (after Cotecchia et al. 2007). Key - 1) colluvial deposits; 2) alluvial deposits; 3) Faeto Flysch stable (a) and landslide debris (b); 4) Red Flysch (SCM soils) with upper bentonite clays (a; BENT soils); 5) strata attitude; 6) landslide features (a-main scarp, b-body); 7) bentonite quarry (a) and spring (b); 8) location of the sampling areas and of the inclinometer (A: scaly clay blocks, B: undisturbed borehole samples and inclinometer, C: bentonite clay blocks); 9) Santa Croce di Magliano village; 10) lines of Sections I and II; 11) sliding surface; 12) landslide body; 13) FAE; 14) RF and bentonite (a) clayey strata, 15) stratigraphic contact.

INTACT SOIL		DISCONTINUITY NATURE			DISCONTINUITY ORIENTATION ¹	DISCONTINUITY GEOMETRY		
Main sediment fraction	Undrained strength ²	Type	Roughness ³	State		Shape ⁴	Continuity ⁴	Intensity ⁵
A	B	C	D	E	F	G	H	I
1 Clay <small>○/*/**+/^</small>	Mudstone	Depositional	Very rough	Fresh <small>○/*/**+/^</small>	Single <small>*+</small>	Planar <small>○/*/**+/+</small>	Continuous ⁺ 	Rare: $<3\text{m}^2/\text{m}^3 - >1\text{m}^3$
2 Silt	Stiff clay [○]	Stress relief <small>**</small>	Rough	Slightly weathered <small>○/*/**+/^</small>	Few	Curved ^{○/*}	Many intersections <small>○/*/**+/^</small> 	Very low: $3-10\text{m}^2/\text{m}^3$ $0.027-1\text{m}^3$
3 Silty clay <small>+^</small>	Firm clay <small>○/*/**+/^</small>	Shear induced <small>○/*/**+/^</small>	Slightly rough	Highly weathered <small>○/*</small>	Many (random) <small>○/**/^</small>	Hinged ^{○/*/^}	Some intersections 	Low: $10-30\text{m}^2/\text{m}^3$ $0.001-0.027\text{m}^3$
4 Clayey silt	Soft clay <small>○/*/**+/^</small>		Smooth <small>○/*/**/^</small>	Iron stained surfaces [○]		Folded ^{○/*/**/^}	Very few intersections 	Medium ⁺ : $30-100\text{m}^2/\text{m}^3$ $27-1000\text{cm}^3$
5 Marly clay			Very smooth <small>○/*</small>	Coated		Conchoid [^]		High ^{**+/^} : $100-300\text{m}^2/\text{m}^3$ $1-27\text{cm}^3$
6			Slickensided <small>○/*/**+/^</small>					Very high ^{○/*/^} : $>300\text{m}^2/\text{m}^3 -$ $<1\text{cm}^3$

¹ With respect to the horizontal direction.

² After Morgenstern & Eigenbrod (1974) and BS 8004 (1986).

³ Sandpaper grade (Fookes & Denness 1969); roughness classification (ISRM 1993).

⁴ After Coffey & Partners in Walker et al. (1987).

⁵ Area of discontinuities per unit volume (m^2/m^3) and/or average size (m^3, cm^3) of the intact peds/blocks (after Fookes & Denness 1969, modified).

Fig. 7 Characterisation chart for fissured clays; in grey are the F-IDs of the clays for which the applicability of the framework has been checked. For the clays in the slopes of reference in the paper, F-IDs: SEN scaly clay (°), SCM scaly clay (*), BENT (**), PD scaly clay I6 (^), PD scaly clay I5-I4 (+).

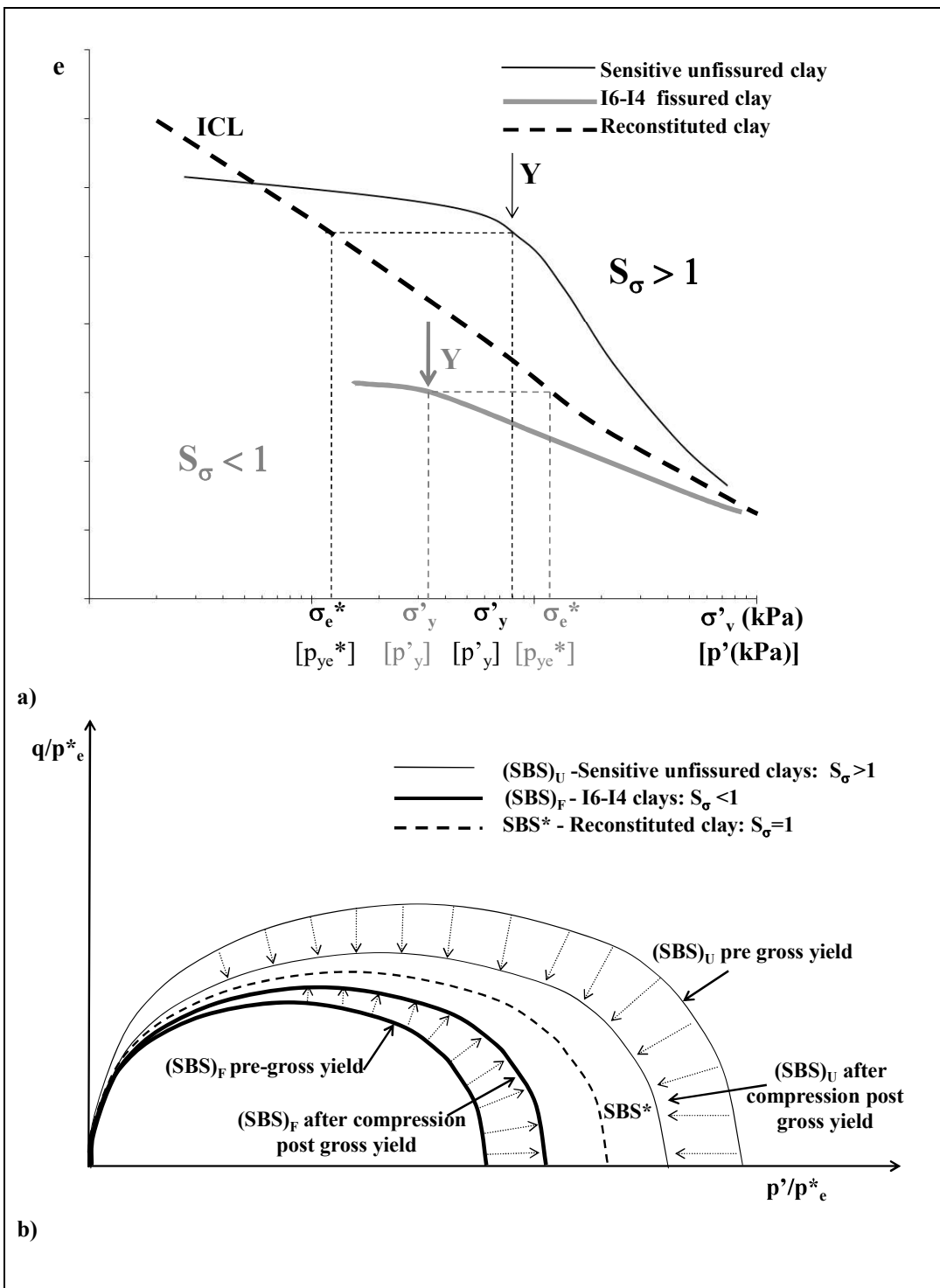


Fig. 8 Natural fissured clay, sensitive unfissured clay and reconstituted clay: framework of a) compression and b) shearing behaviour (after Vitone and Cotecchia 2011, modified)

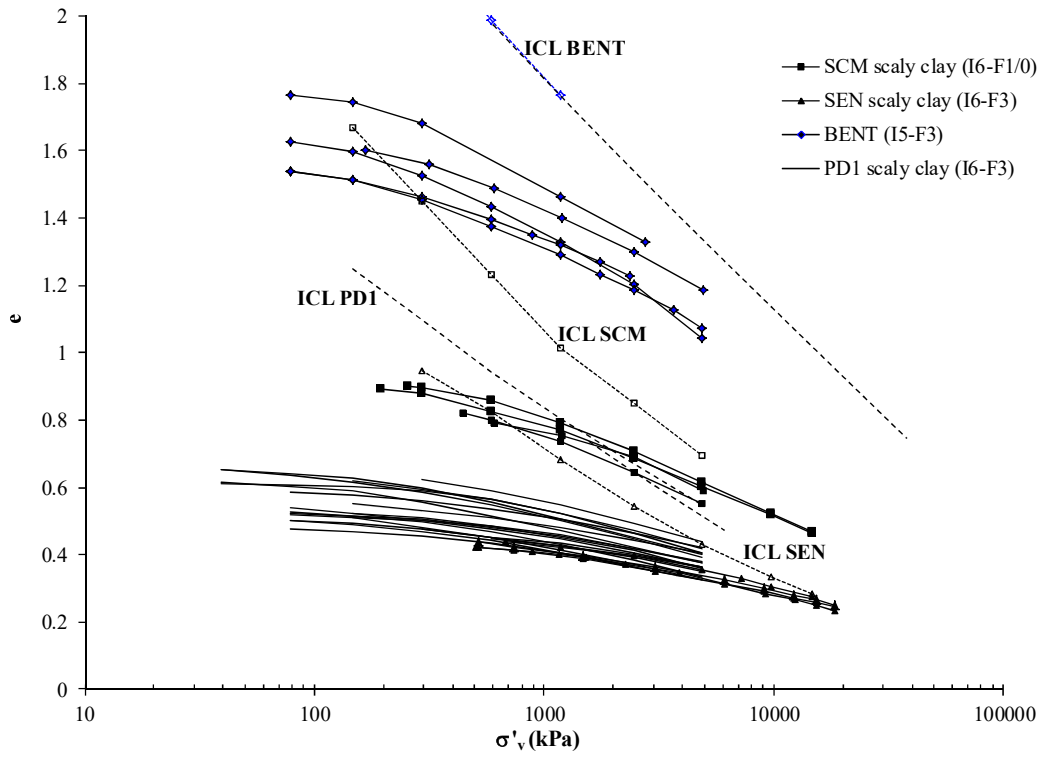


Fig. 9 Natural (continuous lines and full symbols) fissured clays and reconstituted (dashed lines and empty symbols): oedometer compression curves; data from Vitone & Cotecchia (2011) and new data (PD scaly clays).

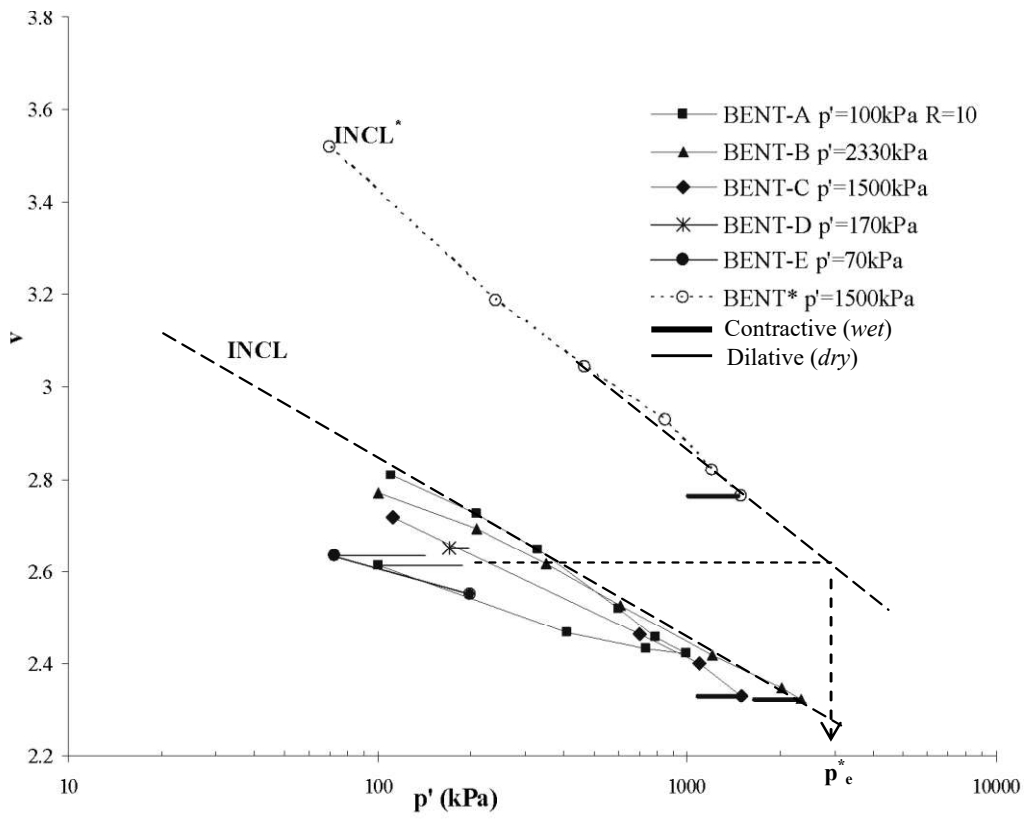


Fig. 10 Natural and reconstituted BENT: isotropic compression and undrained shear state paths.

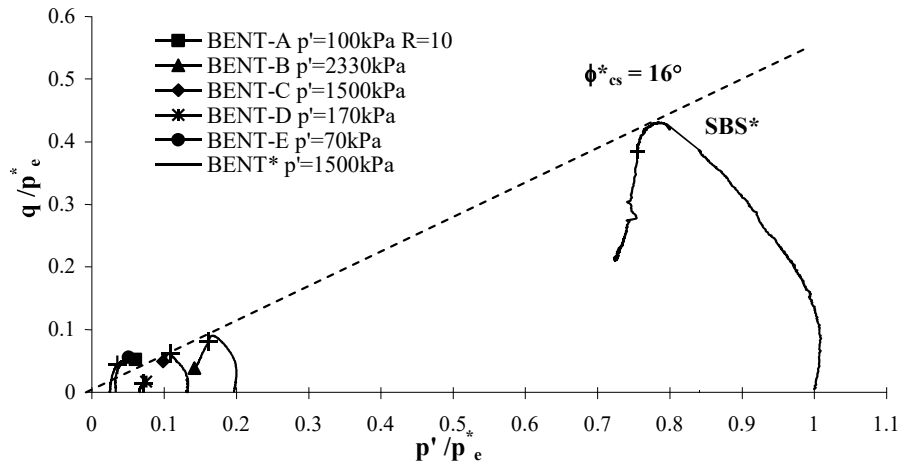


Fig. 11 Natural and reconstituted BENT: undrained stress paths normalized for volume (see Fig. 10).

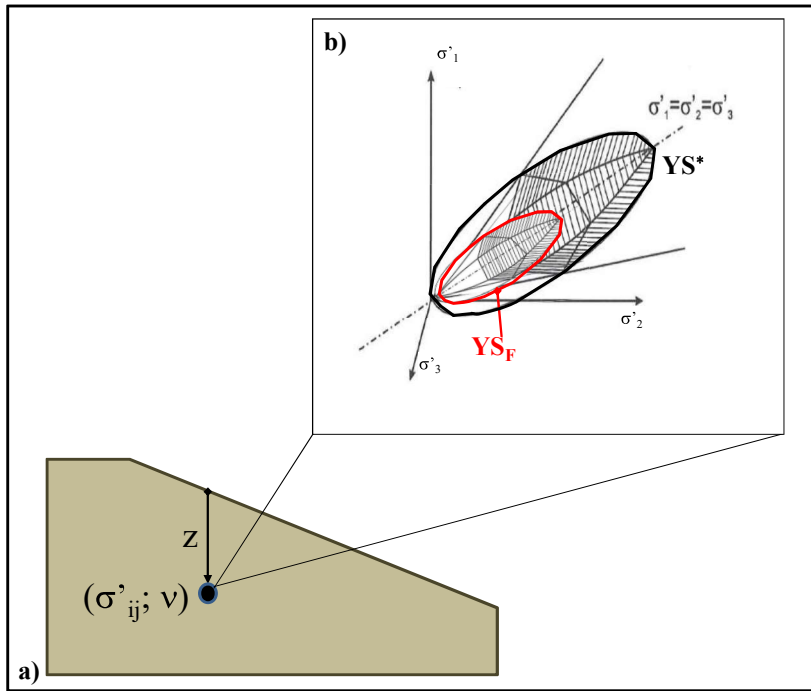


Fig. 12 Conceptual scheme representing the influence of fissuring on the slope stability. In the general stress space (b), the yield surface of the fissured clay, YS_F , and of the reconstituted clay, YS^* , are compared. The asterisk, *, is used for the reconstituted clay.

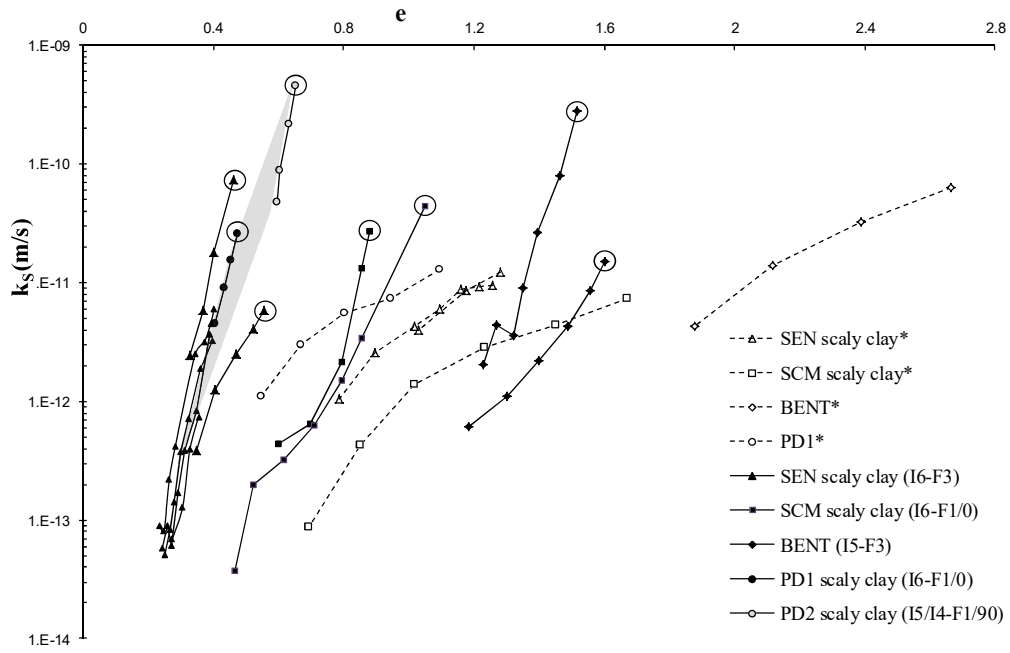


Fig. 13 Reconstituted and natural fissured clays: permeability values measured in the laboratory. Dashed lines refer to the reconstituted clay (*) and circles are used for the k_s - e states of the samples in the slopes. The grey area represents the permeability spindle found for PD1 and PD2 clays.

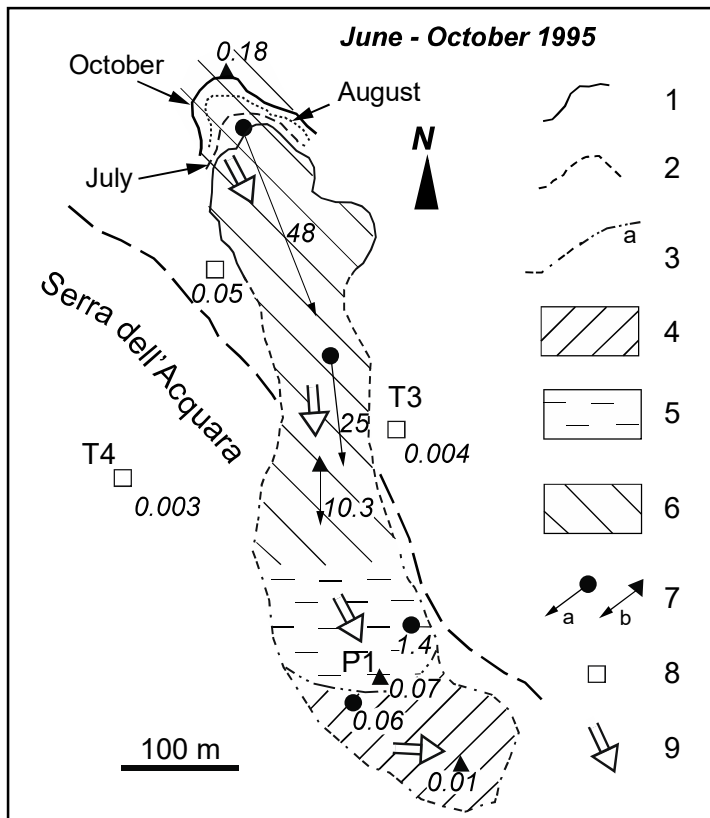


Fig. 14 Horizontal displacement rates (m/month) of the Vadoncello landslide. Key: 1) area A; 2) area B; 3) area C and front of the earth-flow (a); 4) 0.02-0.2 m/month; 5) 0.4-10 m/month; 6) 10-20 m/month; 7) maximum (a) and minimum (b) rates; 8) GPS control stations; 9) average displacement direction (after EEC Project 1996, Santaloia et al. 2001, modified).

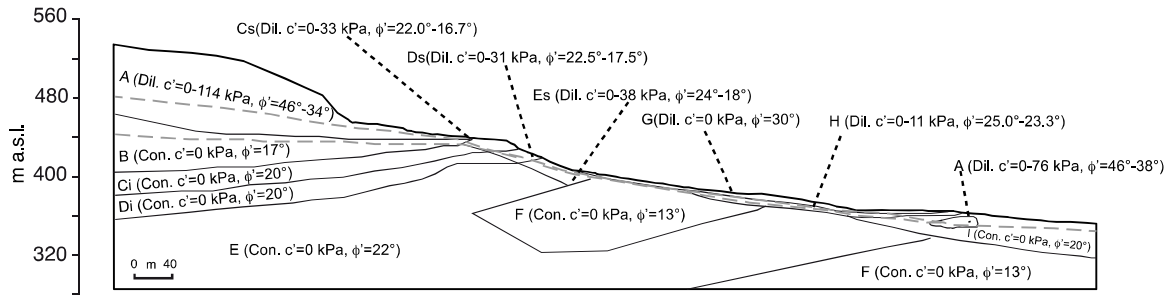


Fig. 15 Vadoncello slope: geotechnical model (Dil: dilative, Con: contractive soil behaviour); the dashed lines represent the water tables of the two seepage domains modelled in the slope (after Cotecchia et al. 2000).

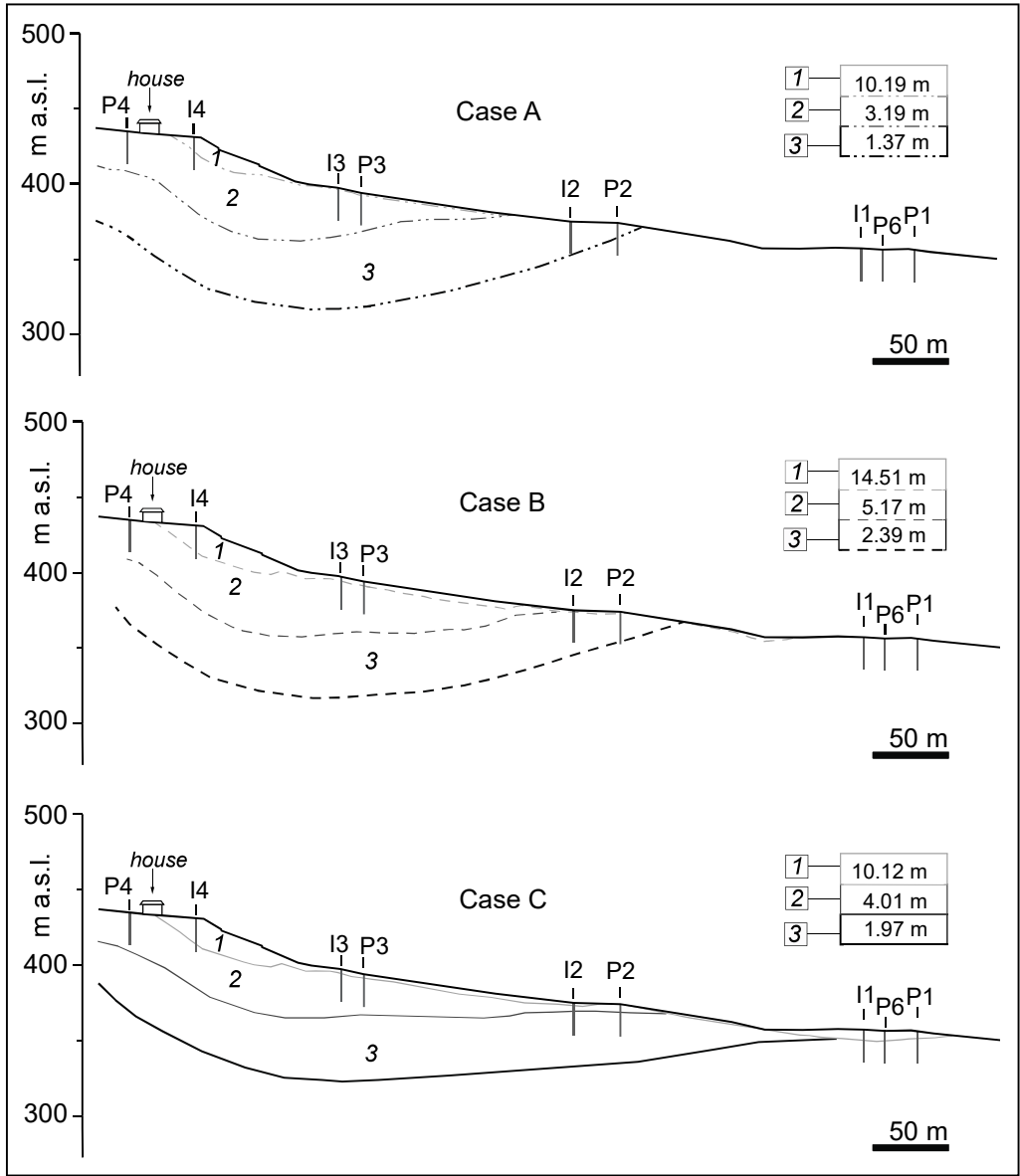


Fig. 16 Vadoncello slope: results of the numerical analysis; areas 1, 2 and 3 are location of quasi-uniform displacement values; the values are shown in the legend for: A - no seepage and no toe translation; B - seepage and no toe translation; C- seepage and toe translation; boreholes equipped with inclinometer (I); boreholes equipped with piezometers (P) (after Cotecchia et al. 2000, modified).

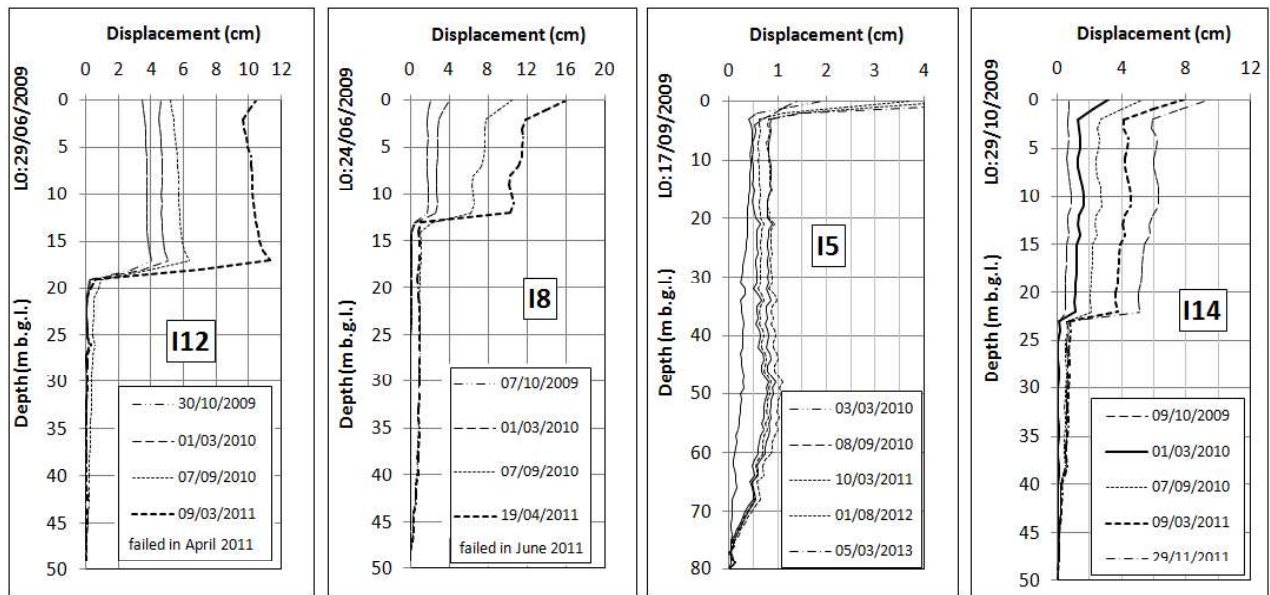


Fig. 17 Cumulative displacement inclinometer profiles within the Pisciola slope. Zero reading in 2009 (L0 in the graphs); location of inclinometers in Fig. 5 (after Cotecchia et al. 2012).

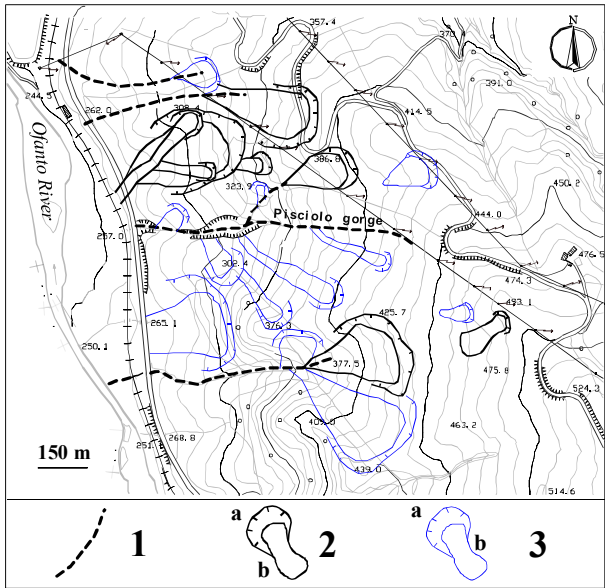


Fig. 18 Geomorphological map of the Pisciole landslide basin (from 1955 aerial photos). Key: (1) deep ditch; (2) active and (3) inactive deep landslides: a-crown, b-body (after Cotecchia et al. 2012).

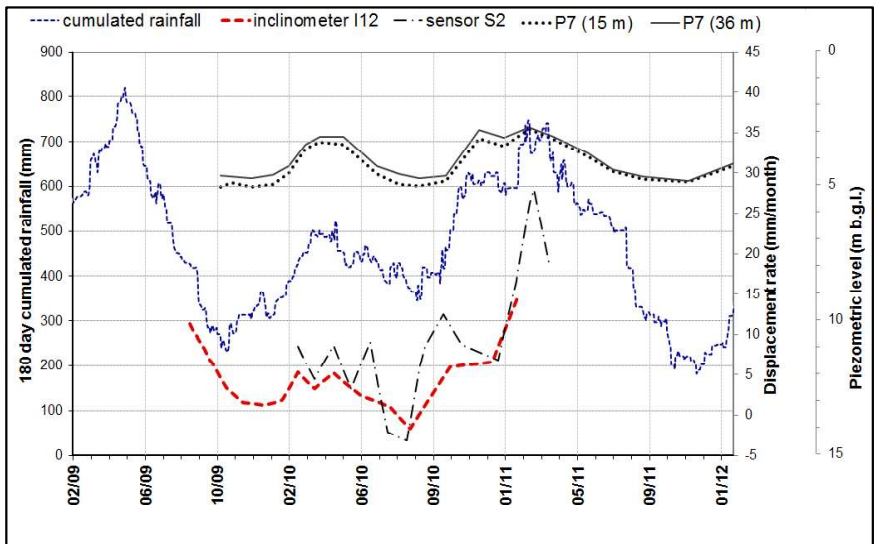


Fig. 19 Displacement rates at 19 m depth down inclinometer I12 and at ground surface (GPS sensor S2); piezometric levels at 15 m and 36 m b.g.l. down borehole P7 and 180 day cumulated rainfall (the location of the monitoring points in Fig. 5).

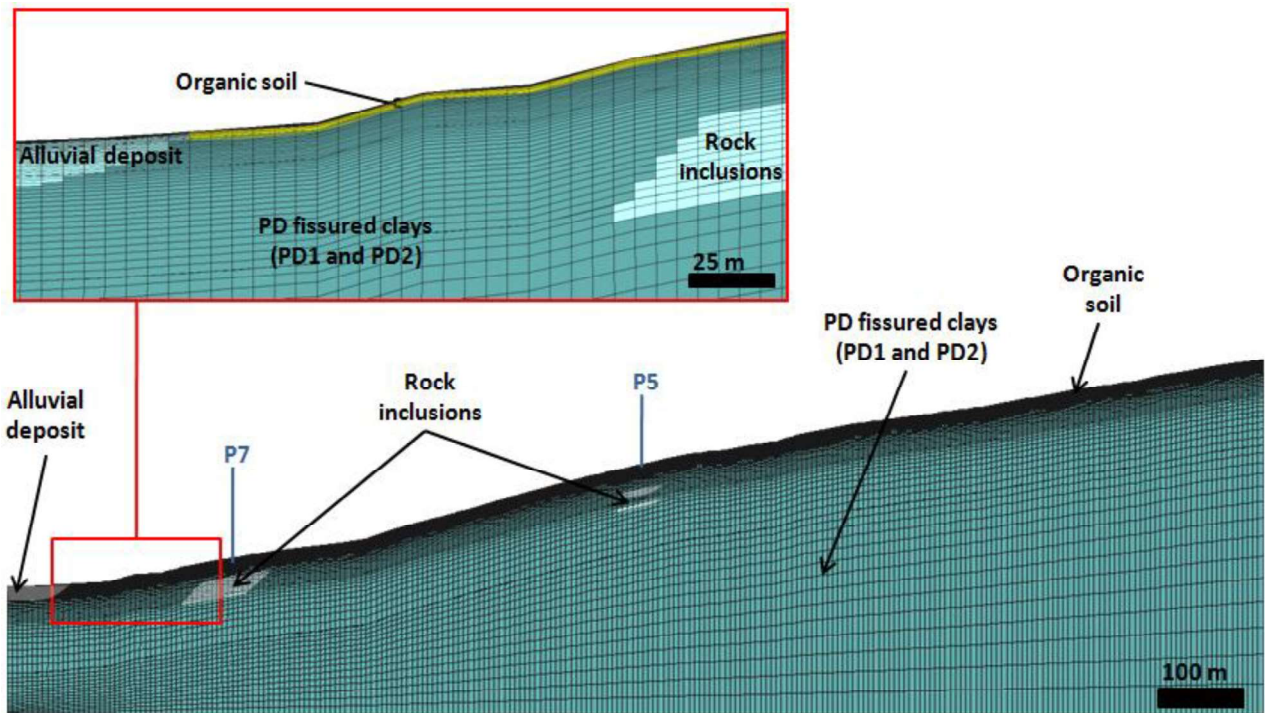


Fig. 20 Numerical model of section II across the Pisciola hillslope; the line of section is shown in Fig. 5b.

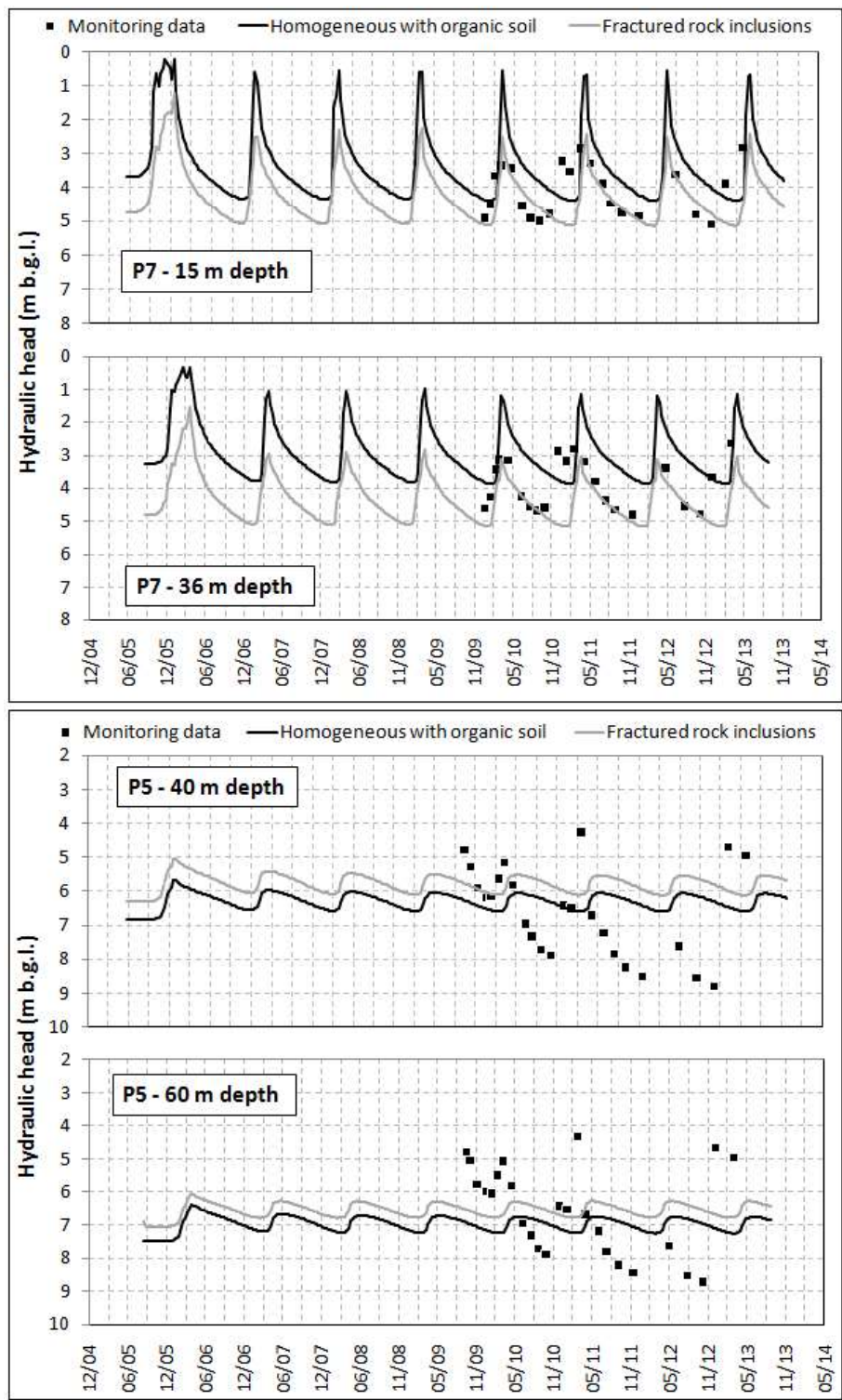


Fig. 21 Measured hydraulic heads (down boreholes P5 and P7) compared to those resulting from the numerical analyses of the model whose numerical mesh is shown in Fig. 20 (section II of the Pisciola hillslope; line of section in Fig. 5b).

Table 1 Clays of reference for the present study: fissuring identities, composition and physical properties. Key: CF: clay fraction; SF: sand fraction; PI: Plasticity index; A: activity; e_0 : initial void ratio; USCS Class: classification according to the Unified Soil Classification System (ASTM 1985)




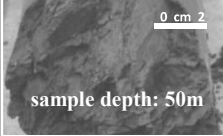
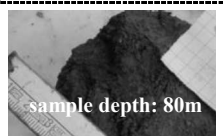
SLOPE	CLAY										
	Name	Fissuring characterisation <i>F-ID</i>	Sampling		Composition and physical properties						
			Type	Depth range (m b.g.l.)	CF %	SF %	PI %	A -	e_0 -	CI -	USCS Class
Santa Croce di Magliano (SCM)	SCM scaly clay	 sample depth: 3m F1-I6	block	3.0	91	9	55	0.6	0.88-1.05	1.1	CH
		A1; B3-4; C3; D4-6; E1-3; F1; G1-4; H2; I6	borehole	54.4	73	-	28	0.4	0.54-0.64	1.9	CH
	BENT	 F3-I5	block	18.0	66	2	86	1.3	1.55-1.79	0.9	CH
		A1; B4; C2-3; D4; E1-2; F3; G1, G4; H2; I5									
Vadoncello (SEN)	SEN scaly clay	 sample depth: 40m F3-I6	borehole	16.0-52.3	36-68	4-18	23-54	0.4-0.8	0.43-0.51	1.0-1.5	CH-CL
		A1; B2-3; C3; D4-6; E1-4; F3; G1-4; H2; I6									
Pisciolo (PI)	PD2	 sample depth: 50m F1-I5/I4	borehole	6.0-80.0	19-55	16-26	24-44	0.5-1.0	0.41-0.69	1.0-1.6	CH
		A1, A3; B3-4; C3; D6; E1-2; F1; G1; H1-2; I5/I4									
	PD1	 sample depth: 80m F3-I6		9.4-80.1	36-70	5-16	38-67	0.6-1.3	0.43-0.81	1.0-1.3	CH
		A1, A3; B3-4; C3; D4, D6; E1-2; F3; G3-5; H2; I6									

Table 2 Values of friction angles of the fissured and reconstituted clays. Key: data from (a) CIU triaxial tests; (b) Bromhead ring shear tests; (c) reversal direct shear tests; n.d. data not determined

SOIL TYPE	SHEAR TEST RESULTS
SE scaly clay	$\phi'_{\text{peak}} \approx 18.5^\circ\text{-}20.5^\circ$ (<i>dry</i> side, $R \approx 3$) – (a) $\phi'_{\text{post-peak}} = 12^\circ\text{-}15^\circ$ – (a) $\phi'_r \approx 5^\circ$ – (b) $\phi^*_{\text{cs}} \approx 19^\circ$ – (a)
SCM scaly clay	$\phi'_{\text{peak}} \approx 13^\circ\text{-}22^\circ$ (<i>dry</i> side, $R \approx 2.5\text{-}20$) – (a) $\phi'_{\text{post-peak}} = 9^\circ\text{-}12^\circ$ – (a) $\phi'_r \leq 9^\circ$ – (c) $\phi^*_{\text{cs}} \approx 18^\circ$ – (a)
BENT	$\phi'_{\text{peak}} \approx 16^\circ\text{-}28^\circ$ (<i>dry</i> side, $R \approx 3\text{-}10$) – (a) $\phi'_{\text{post-peak}} = 12^\circ\text{-}27^\circ$ – (a) $\phi'_r \approx 5^\circ$ – (b) $\phi^*_{\text{cs}} \approx 16^\circ$ – (a)
PD1 and PD2 scaly clay	$\phi'_{\text{peak}} \approx 21^\circ\text{-}25^\circ$ (<i>dry</i> side, $R \approx 3\text{-}10$) – (a) $\phi'_{\text{post-peak}} = 13^\circ\text{-}20^\circ$ – (a) $\phi'_r \approx \text{n.d.}$ $\phi^*_{\text{cs}} \approx 18^\circ$ – (a)

Fig. 1
[Click here to download Figure: Fig1 Final.eps](#)

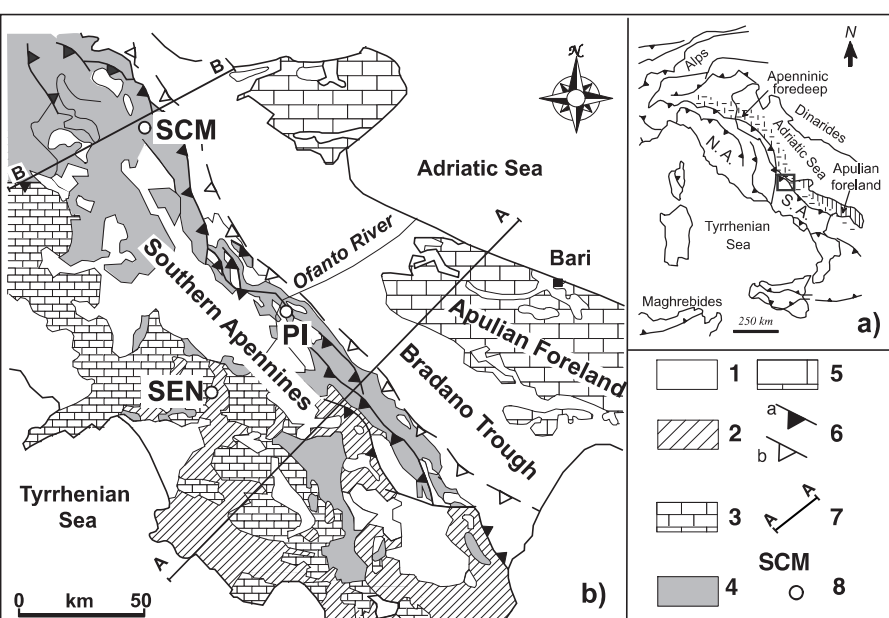


Fig. 2
[Click here to download Figure: Fig2 Final.eps](#)

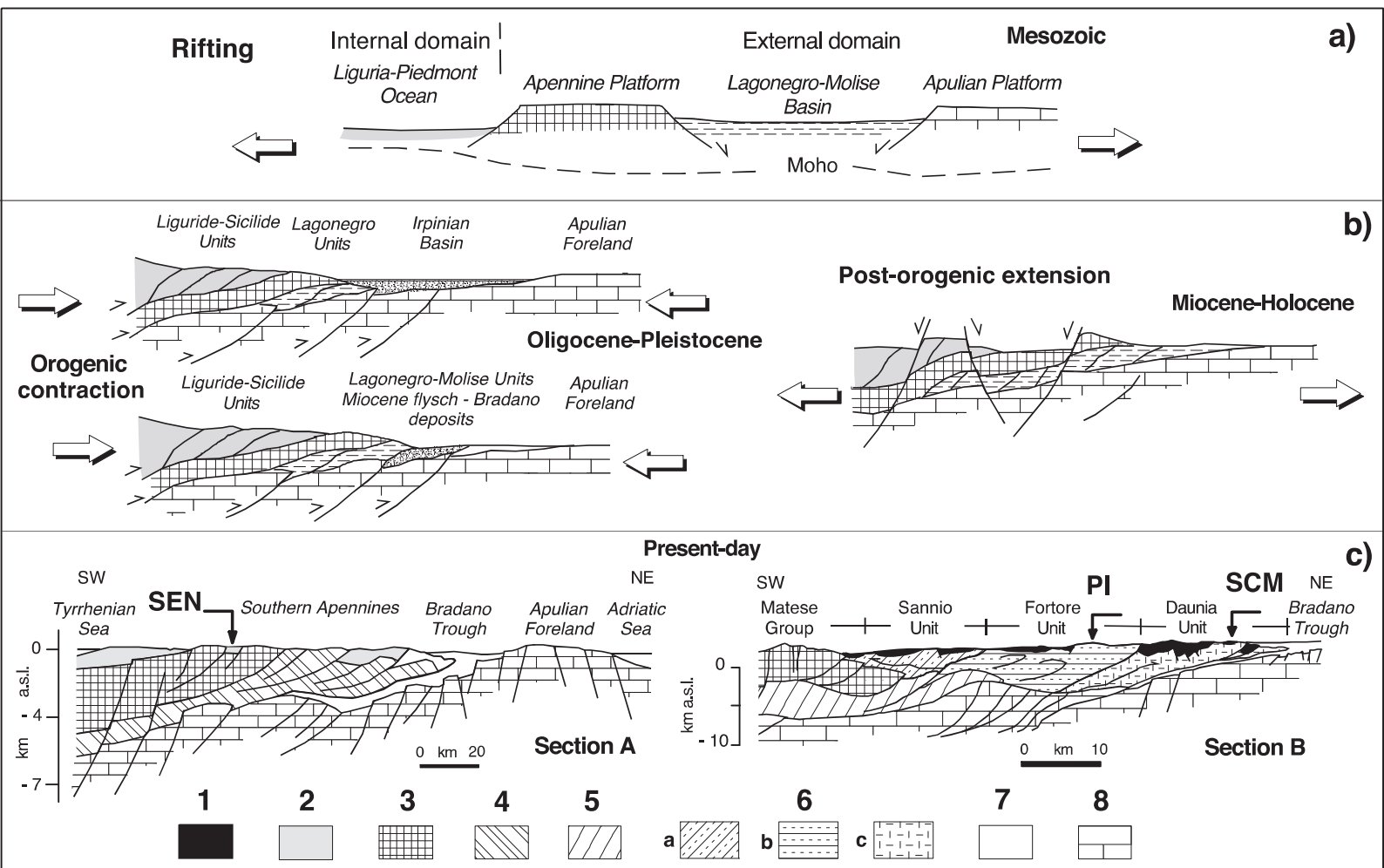


Fig. 3
[Click here to download Figure: Fig3.eps](#)

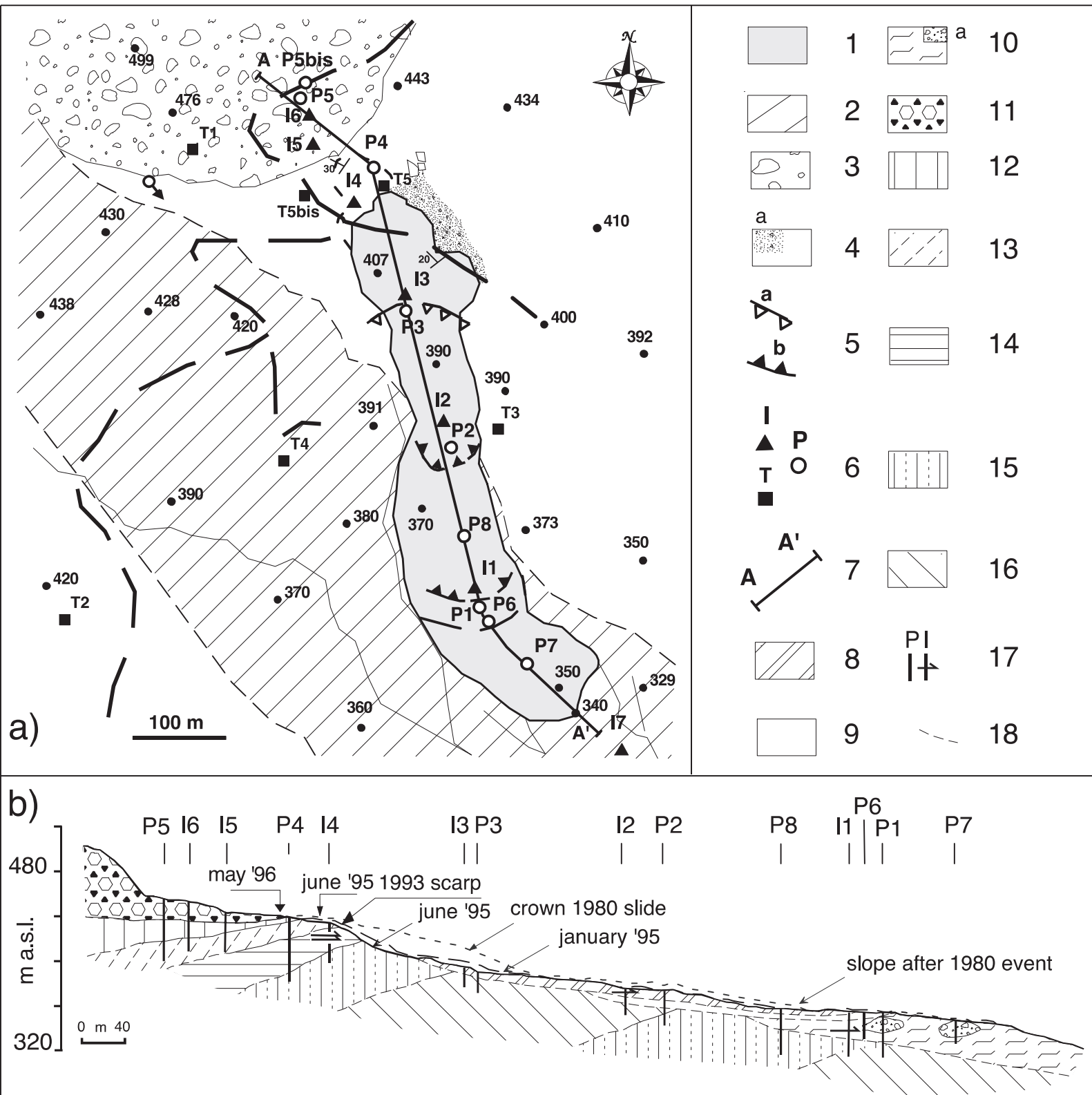


Fig. 4

[Click here to download Figure: Fig4 Final.eps](#)

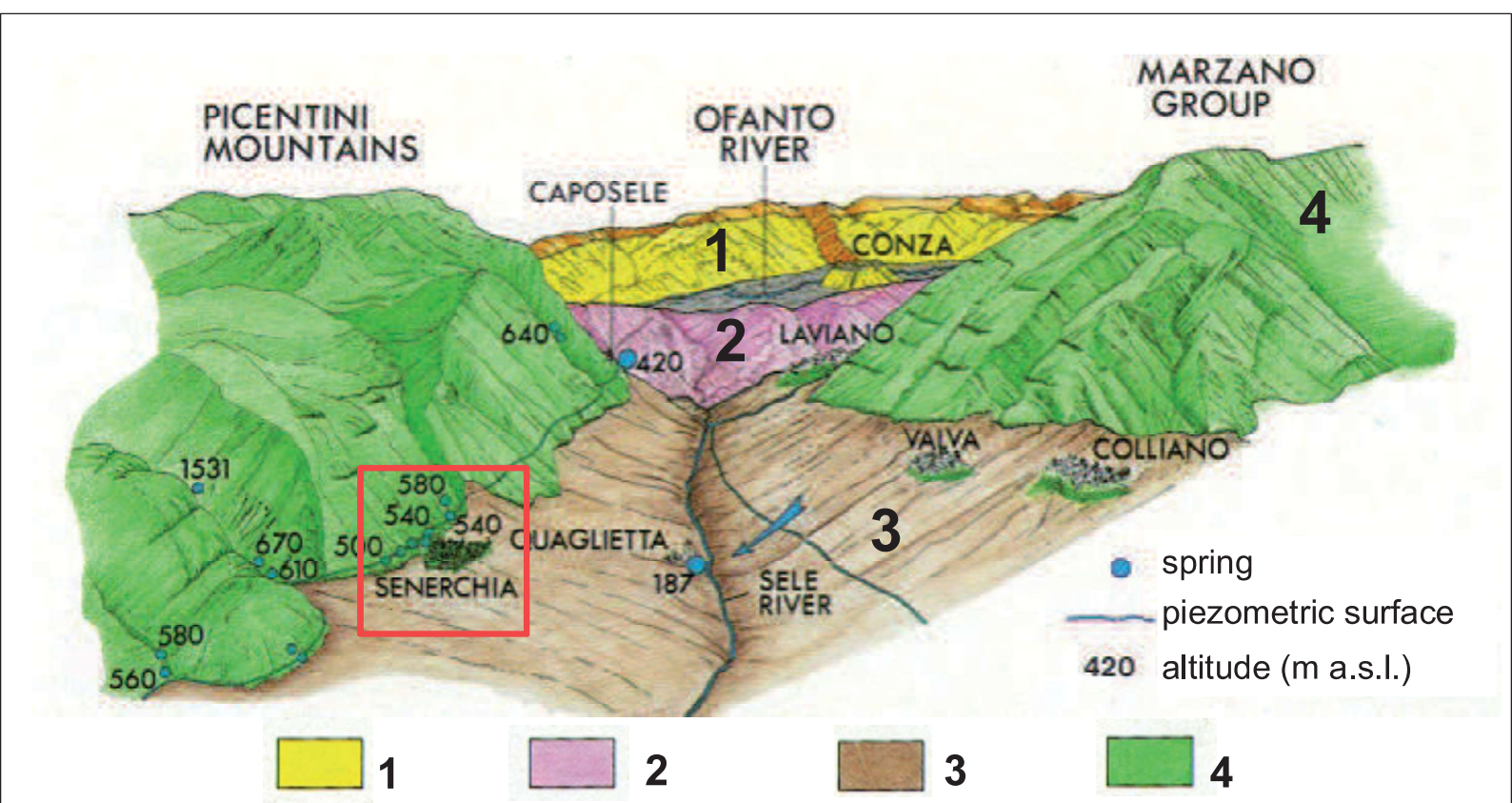


Fig. 5
[Click here to download Figure: Fig5 Final.eps](#)

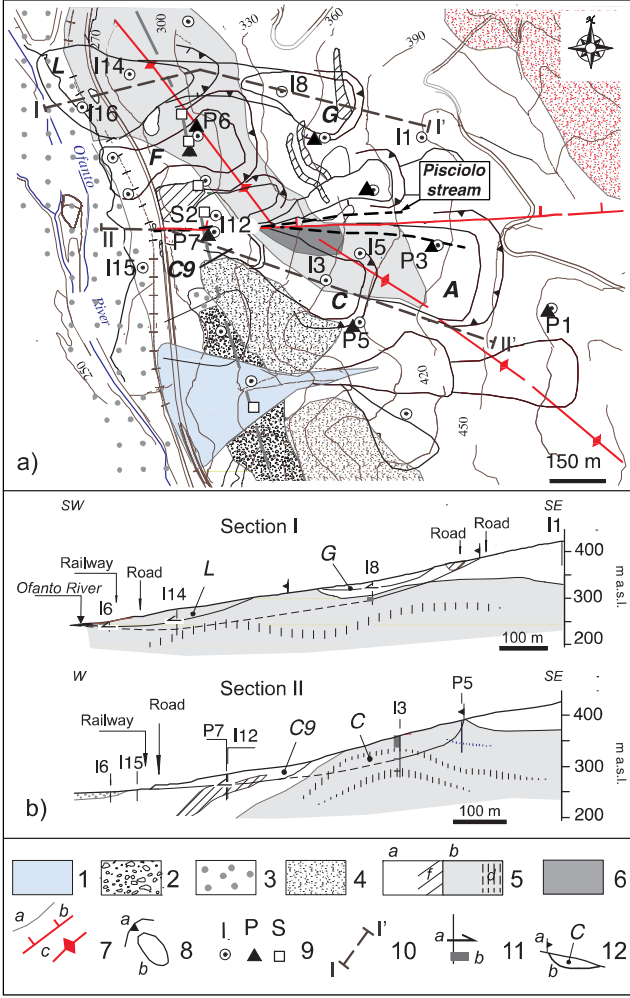


Fig. 6

[Click here to download Figure: Fig6 Final.eps](#)

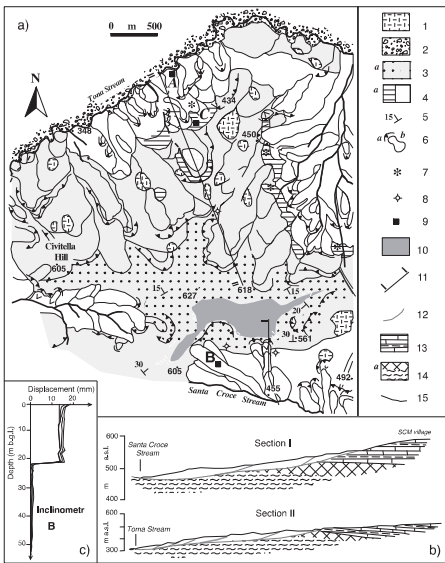


Fig. 7
[Click here to download high resolution image](#)

INTACT SOIL		DISCONTINUITY NATURE			DISCONTINUITY ORIENTATION ¹	DISCONTINUITY GEOMETRY		
Main sediment fraction	Undrained strength ²	Type	Roughness ³	State		Shape ⁴	Continuity ⁴	Intensity ⁵
A	B	C	D	E	F	G	H	I
1 Clay ^{0/1/2/3/4/5/6}	Mudstone	Depositional	Very rough	Fresh ^{0/1/2/3/4/5/6}	Single ⁴⁺	Planar ^{0/1/2/3/4/5/6}	Continuous ⁺	Rare: <3m ² /m ³ >1m ³
2 Silt	Stiff clay ⁰	Stress relief ⁺⁺	Rough	Slightly weathered ^{0/1/2/3/4/5/6}	Few	Curved ^{0/1/2}	Many intersections ^{0/1/2/3/4/5/6}	Very low: 3-10 m ² /m ³ 0.027-1 m ³
3 Silty clay ⁺⁺	Firm clay ^{0/1/2/3/4/5/6}	Shear induced ^{0/1/2/3/4/5/6}	Slightly rough	Highly weathered ^{0/1/2}	Many (random) ^{0/1/2/3/4/5/6}	Hinged ^{0/1/2/3/4}	Some intersections	Low: 10-30 m ² /m ³ 0.001-0.027 m ³
4 Clayey silt	Soft clay ^{0/1/2/3/4/5/6}		Smooth ^{0/1/2/3/4/5/6}	Iron stained surfaces ⁰		Folded ^{0/1/2/3/4/5/6}	Very few intersections	Medium ⁺ : 30-100 m ² /m ³ 27-1000 cm ³
5 Marly clay			Very smooth ^{0/1/2}	Coated		Conchoid ⁺		High ^{0/1/2/3/4/5/6} : 100-300 m ² /m ³ 1-27 cm ³
6			Slickensided ^{0/1/2/3/4/5/6}					Very high ^{0/1/2/3/4/5/6} : >300m ² /m ³ - <1cm ³

¹ With respect to the horizontal direction.

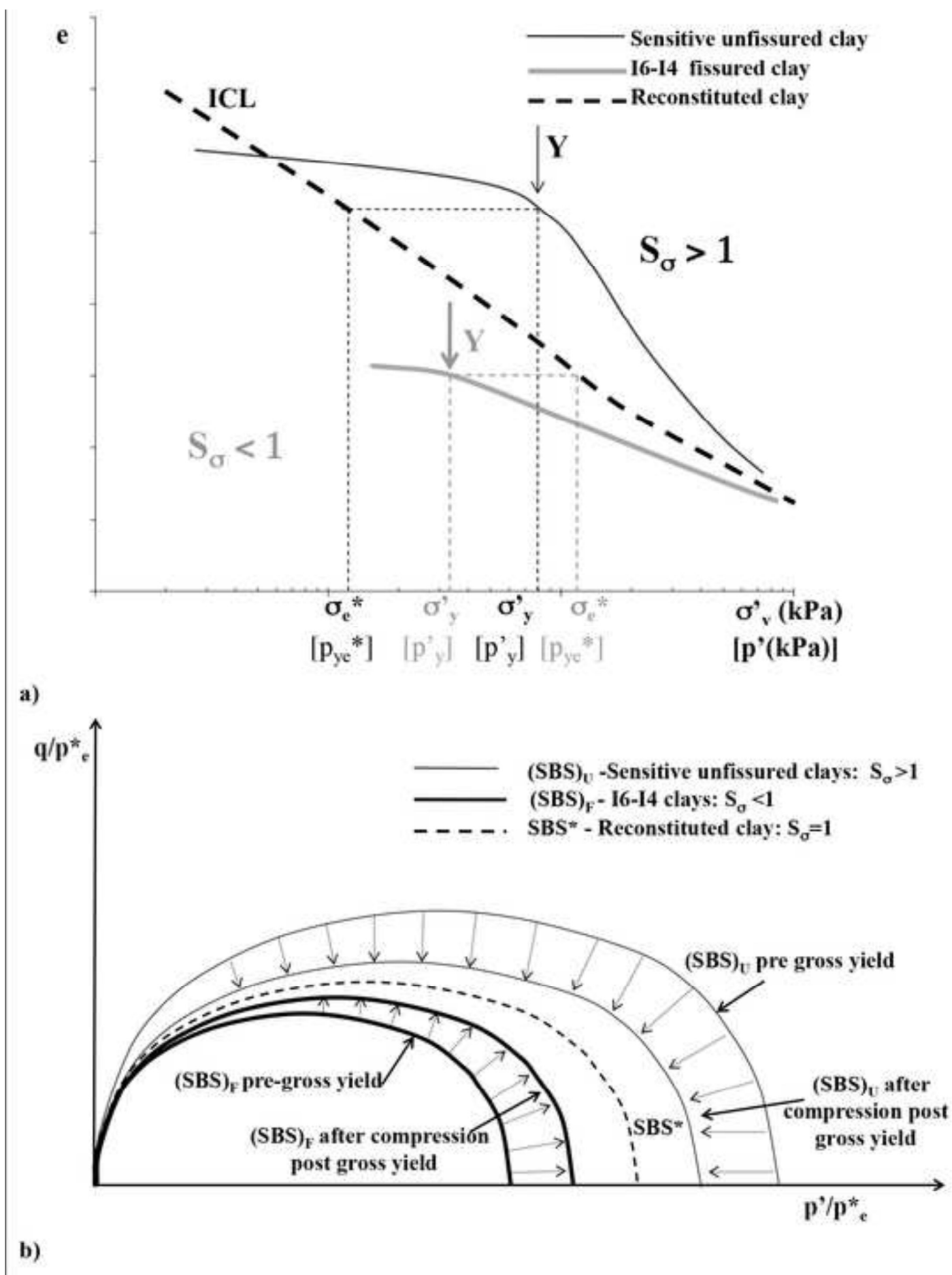
² After Morgenstern & Eigenbrod (1974) and BS 8004 (1986).

³ Sandpaper grade (Fookes & Denness 1969); roughness classification (ISRM 1993).

⁴ After Coffey & Partners in Walker et al. (1987).

⁵ Area of discontinuities per unit volume (m²/m³) and/or average size (m³, cm³) of the intact pedo/blocks (after Fookes & Denness 1969, modified).

Fig. 8
[Click here to download high resolution image](#)



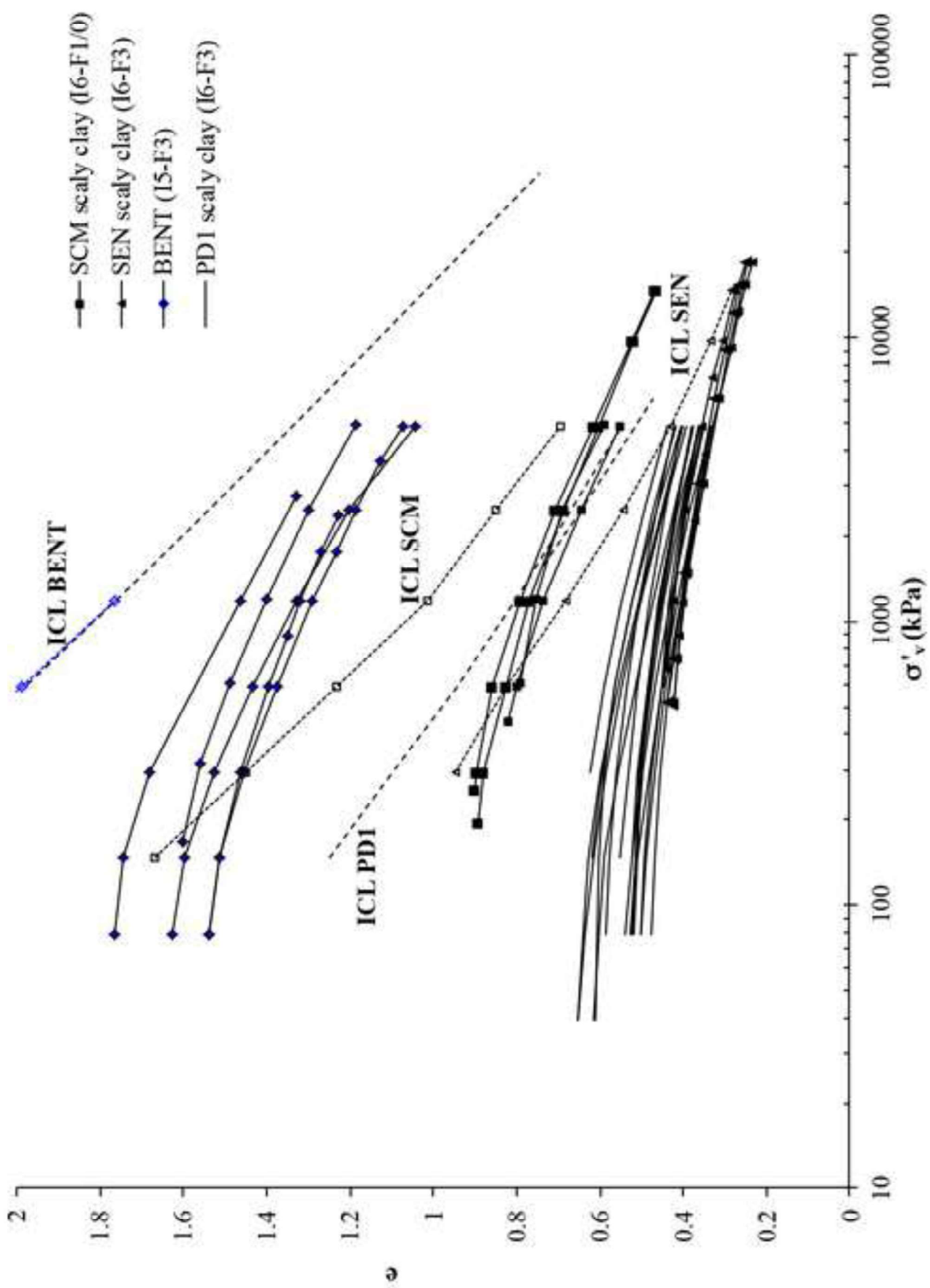


Fig. 9
[Click here to download high resolution image](#)

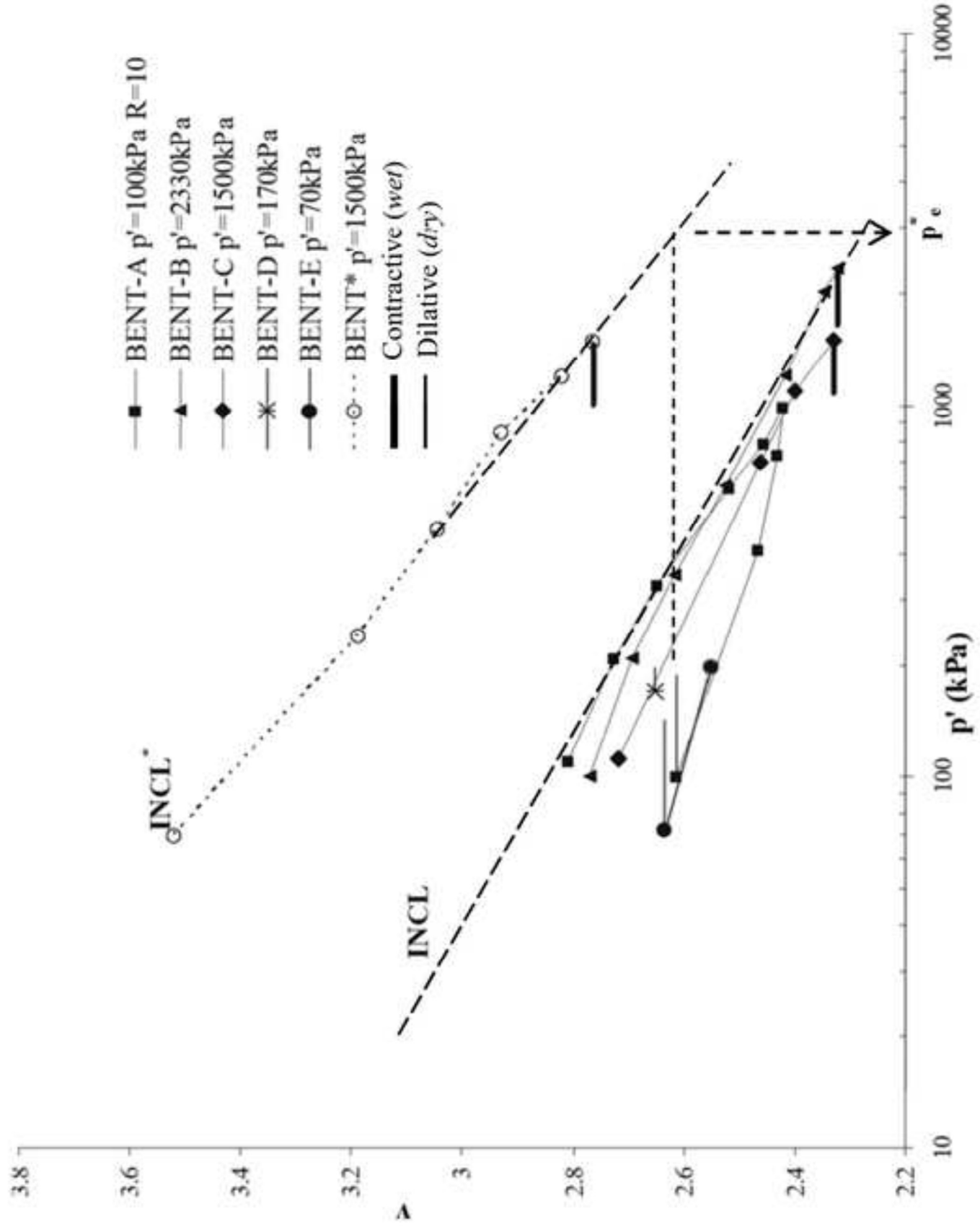


Fig. 10
[Click here to download high resolution image](#)

Fig. 11
[Click here to download high resolution image](#)

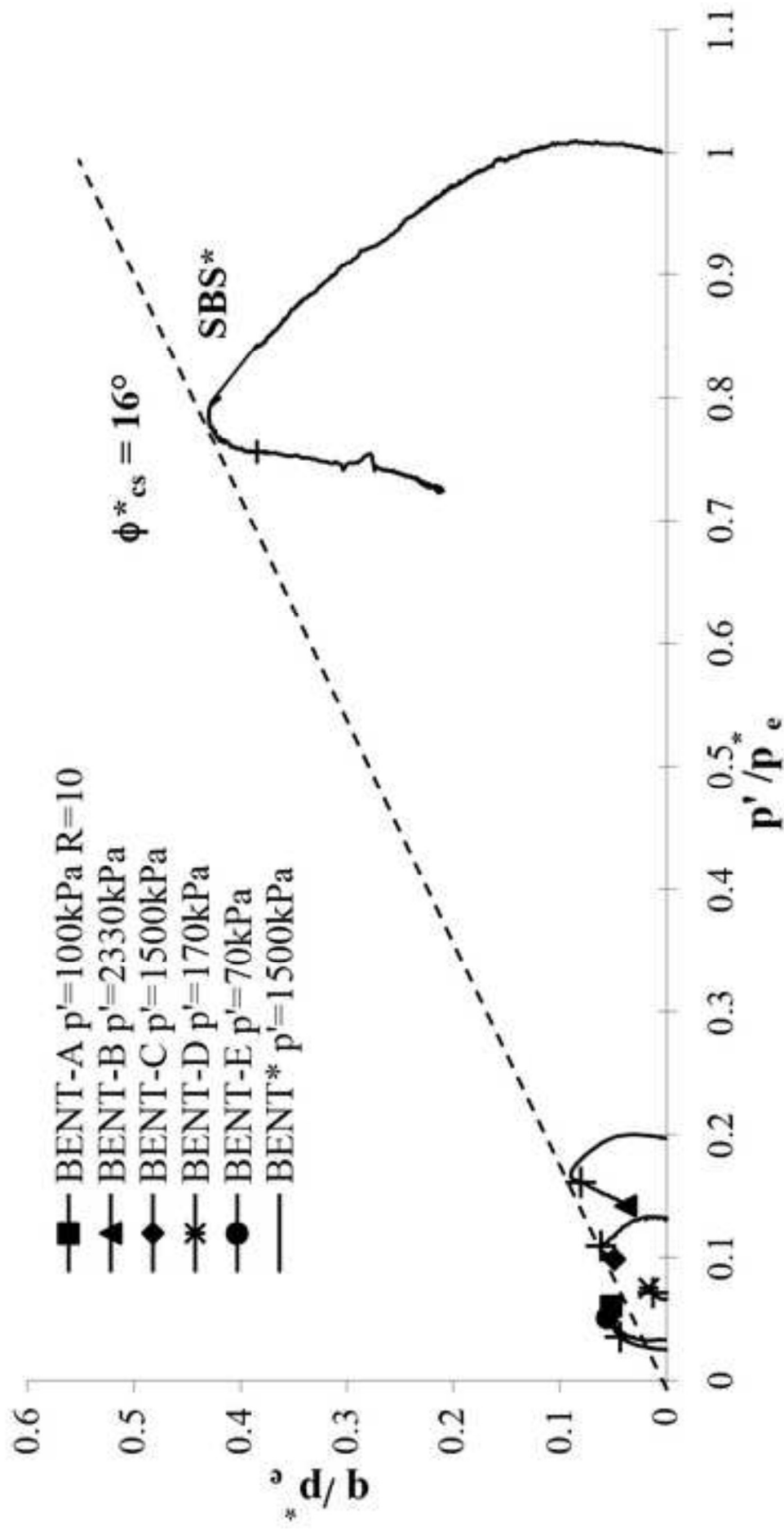


Fig. 12
[Click here to download high resolution image](#)

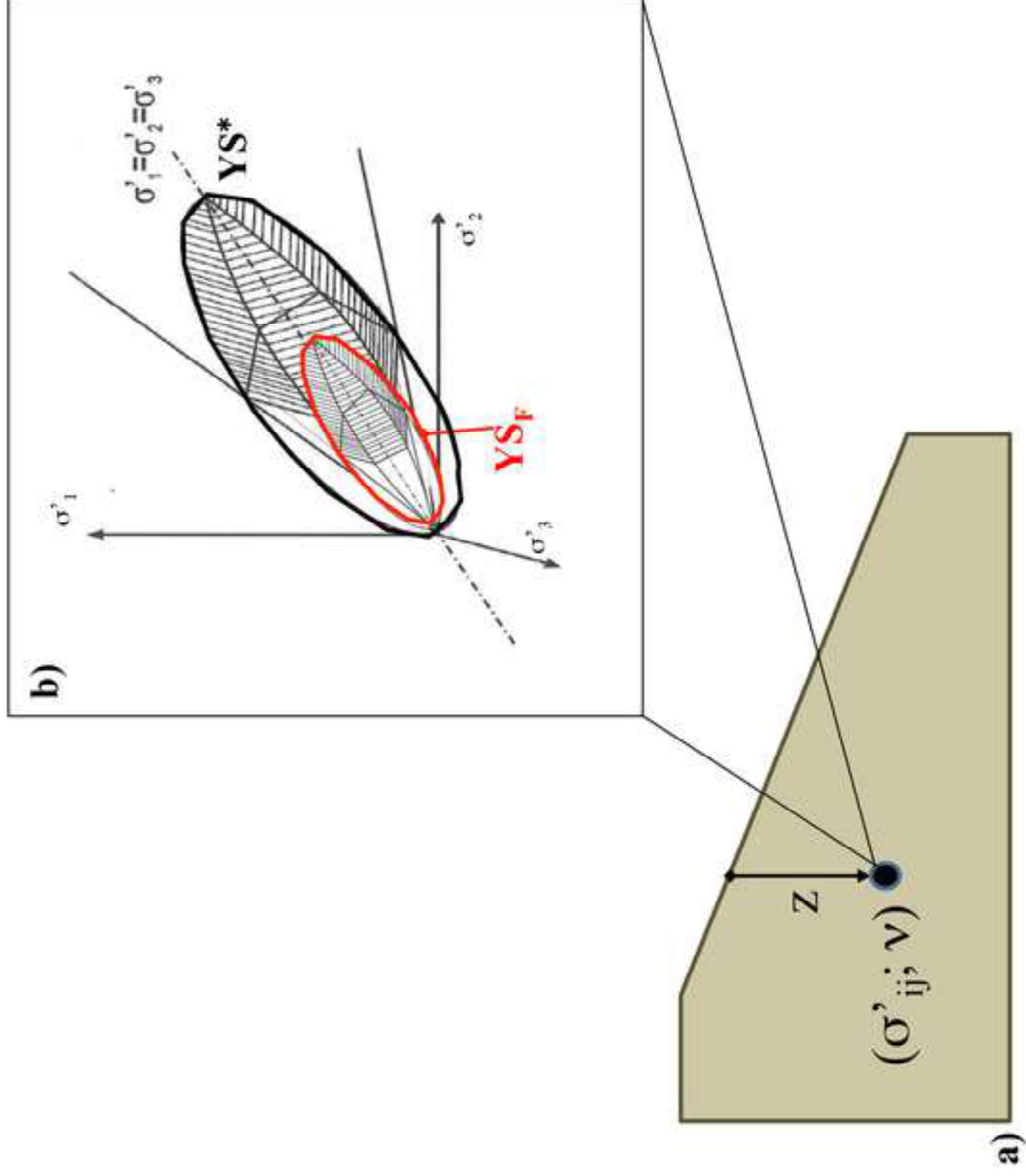


Fig. 13
[Click here to download high resolution image](#)

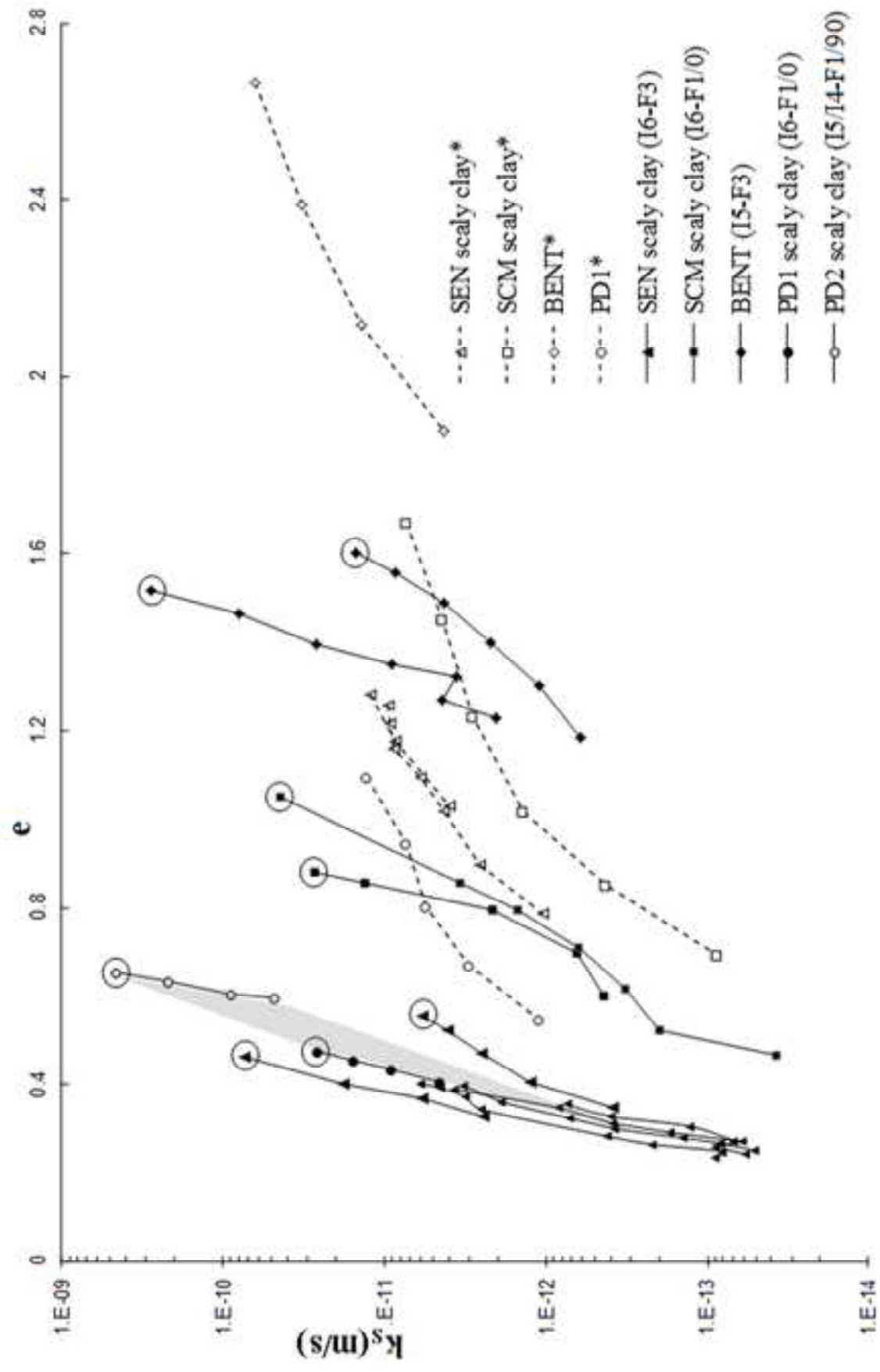


Fig. 14
[Click here to download Figure: Fig14 Final.eps](#)

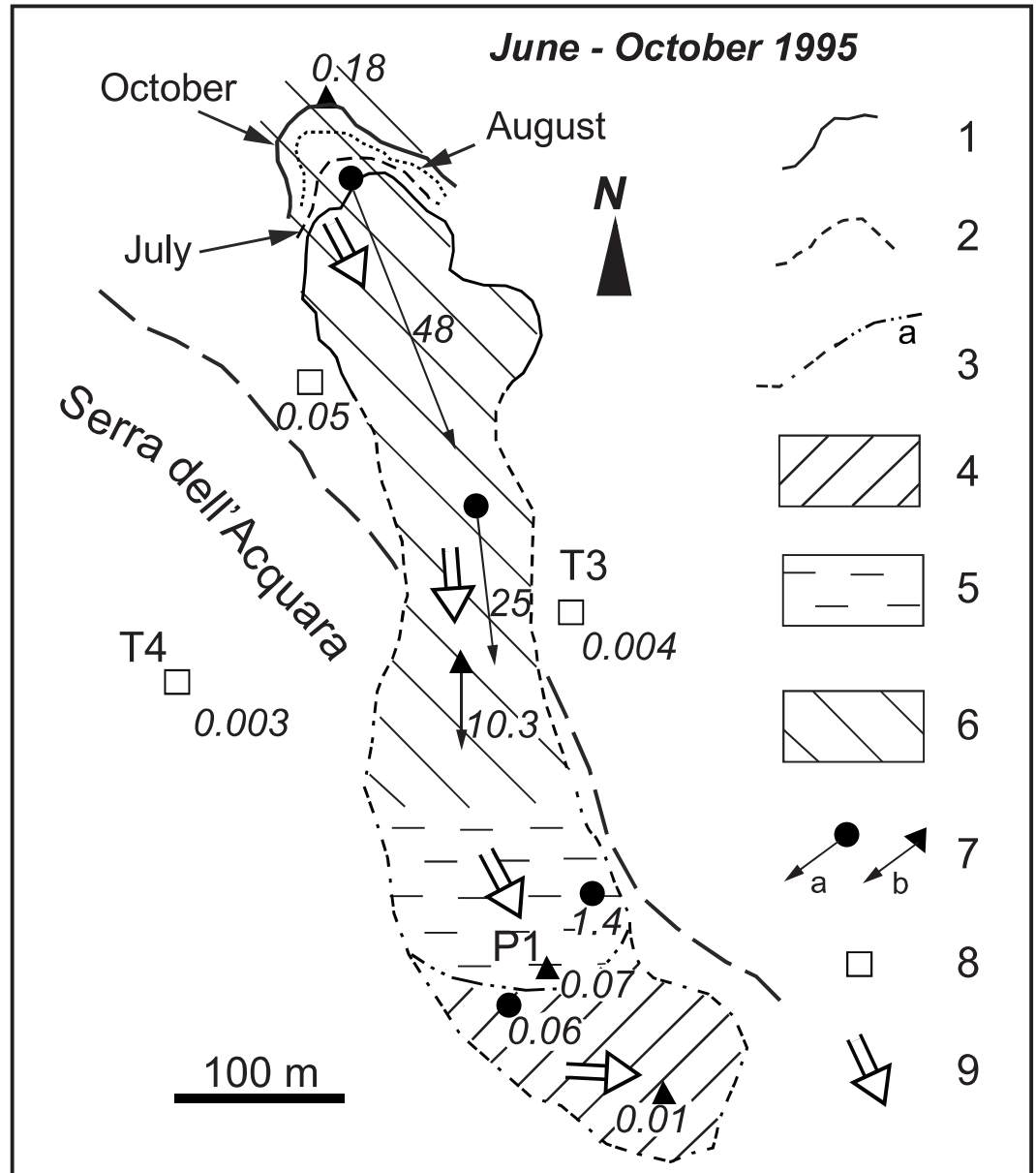


Fig. 15

[Click here to download Figure: Fig15 Final.eps](#)

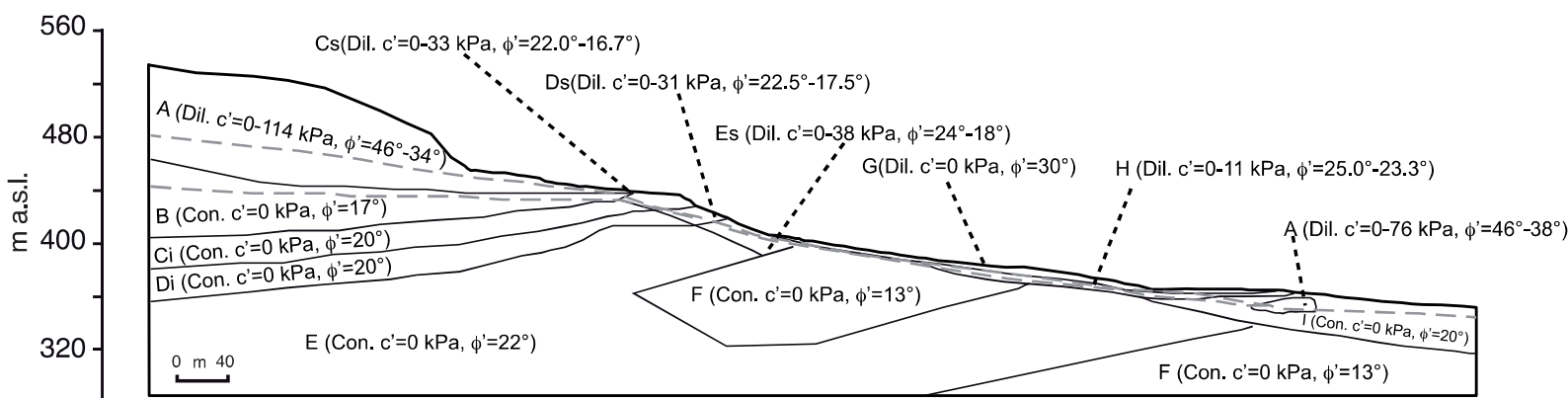


Fig. 16
[Click here to download Figure: Fig16 Final.eps](#)

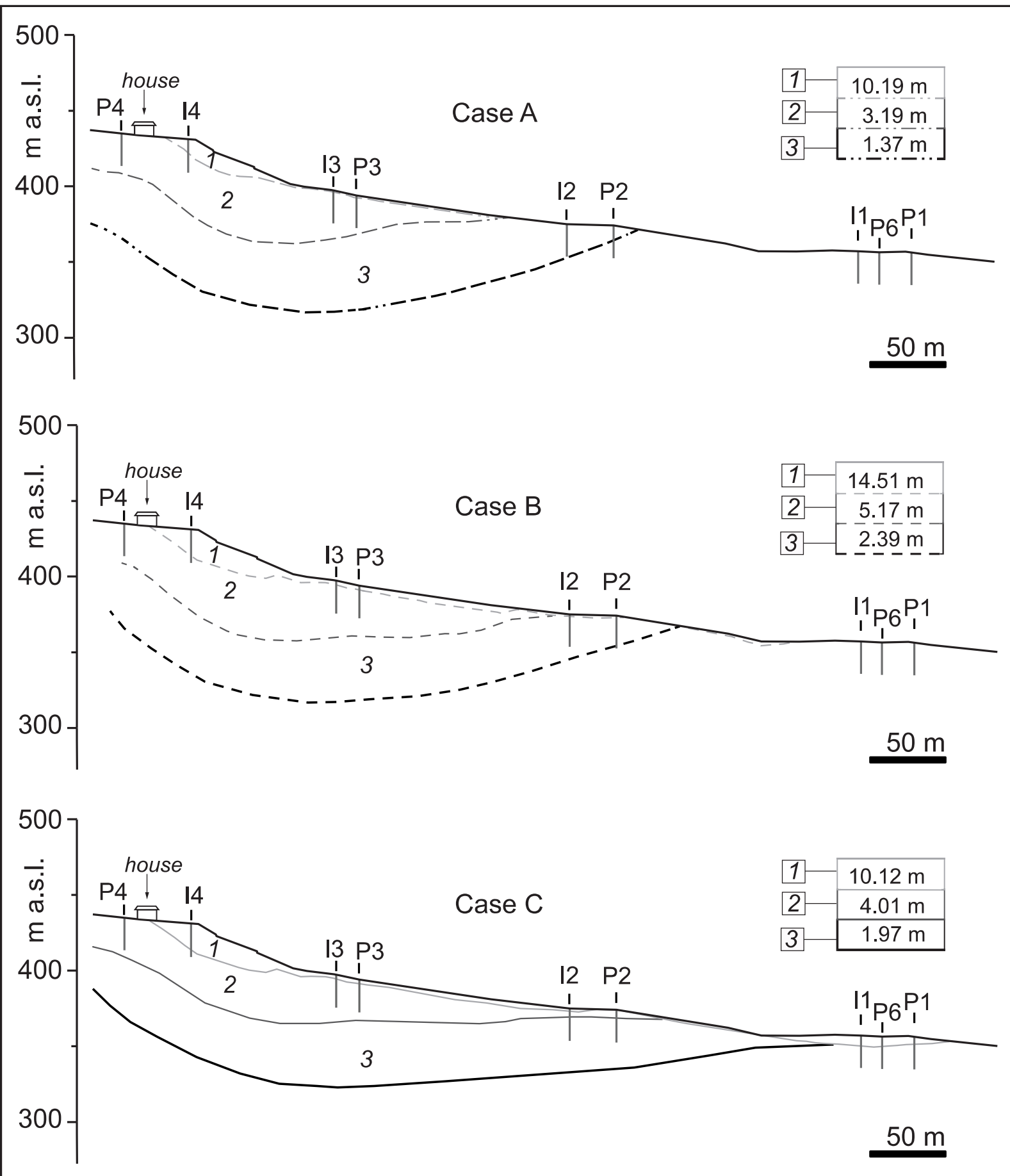


Fig. 17
[Click here to download high resolution image](#)

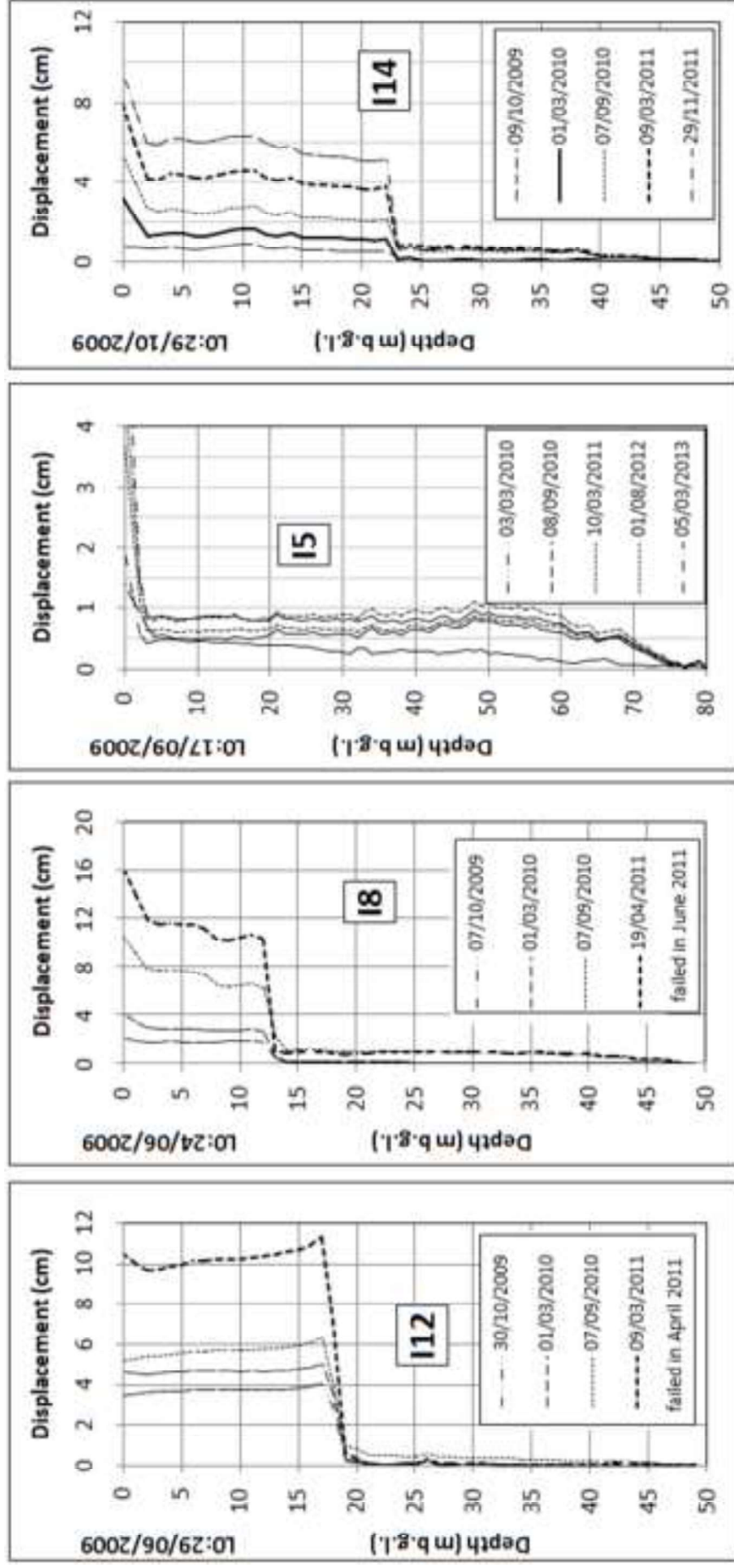


Fig. 18
[Click here to download Figure: Fig18 Final.eps](#)

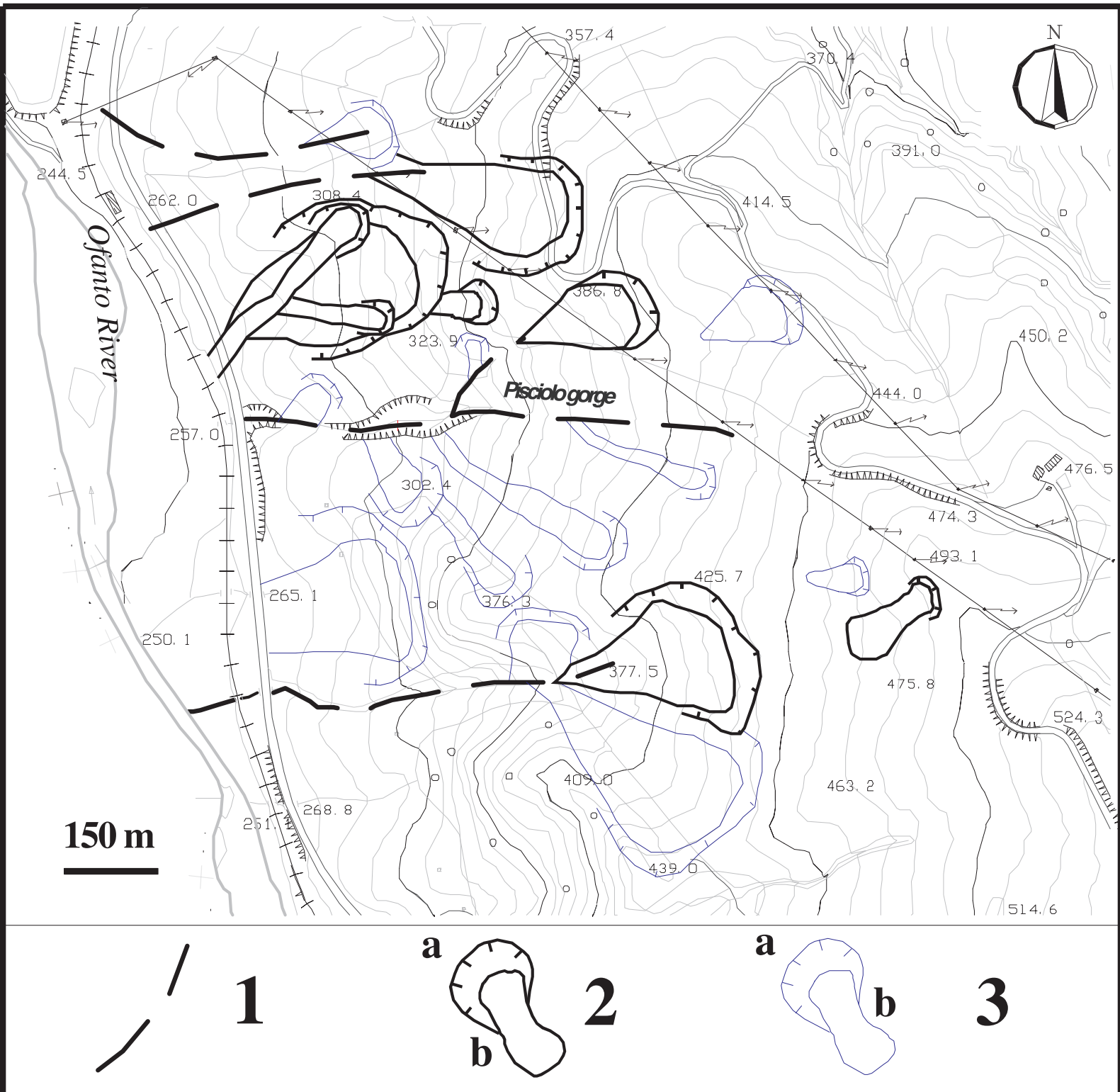


Fig. 19

[Click here to download Figure: Fig19.eps](#)

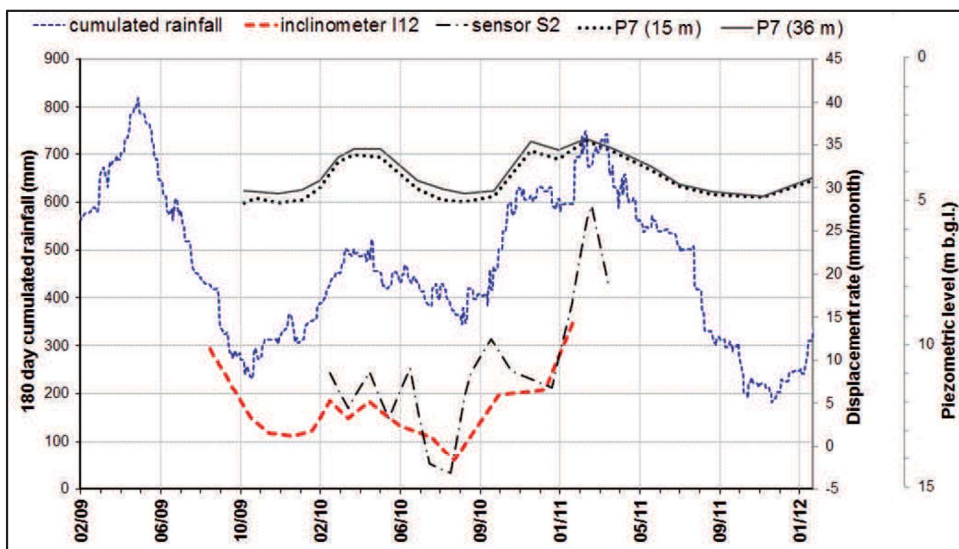


Fig. 20
[Click here to download high resolution image](#)

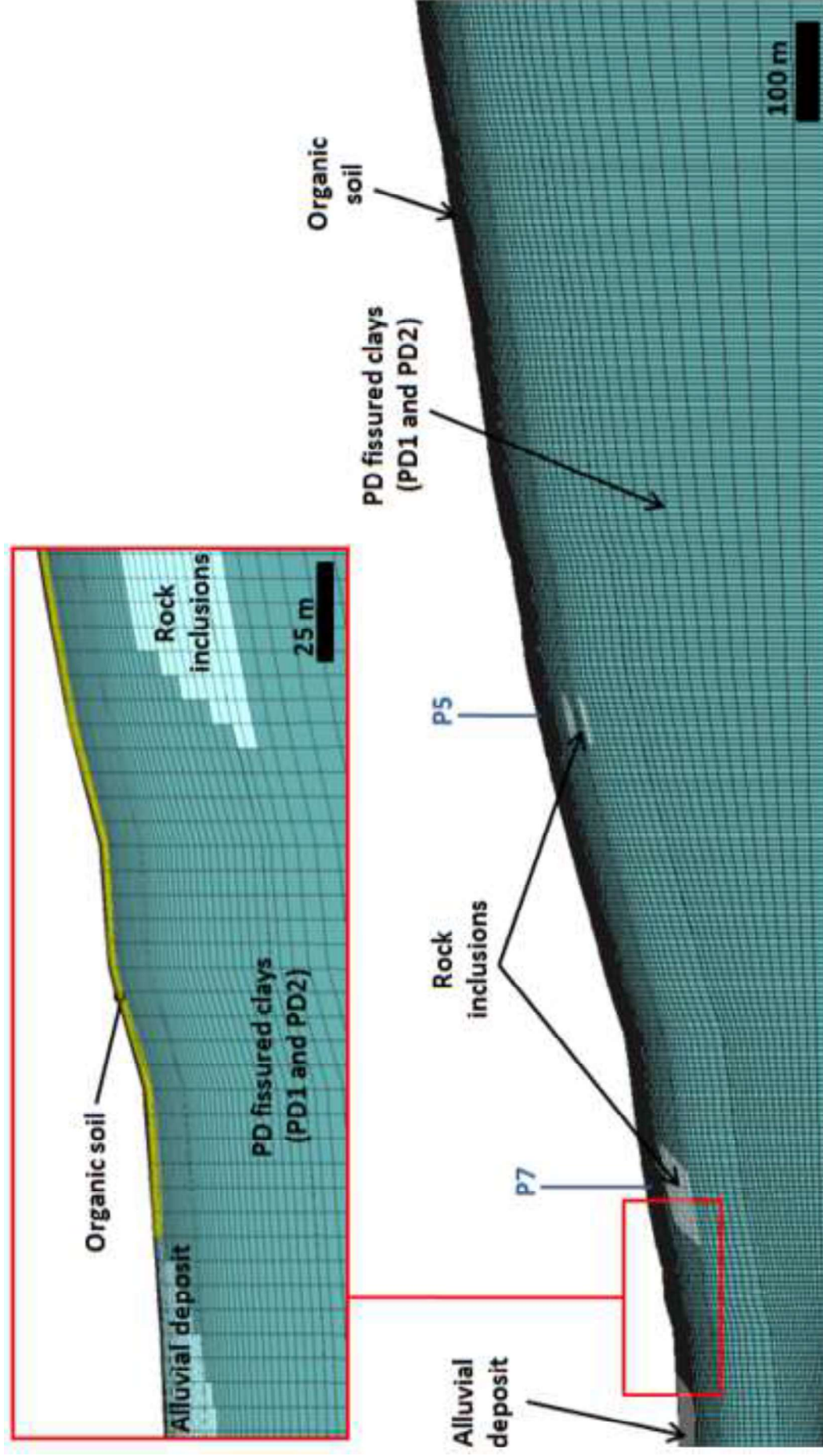


Fig. 21
[Click here to download high resolution image](#)

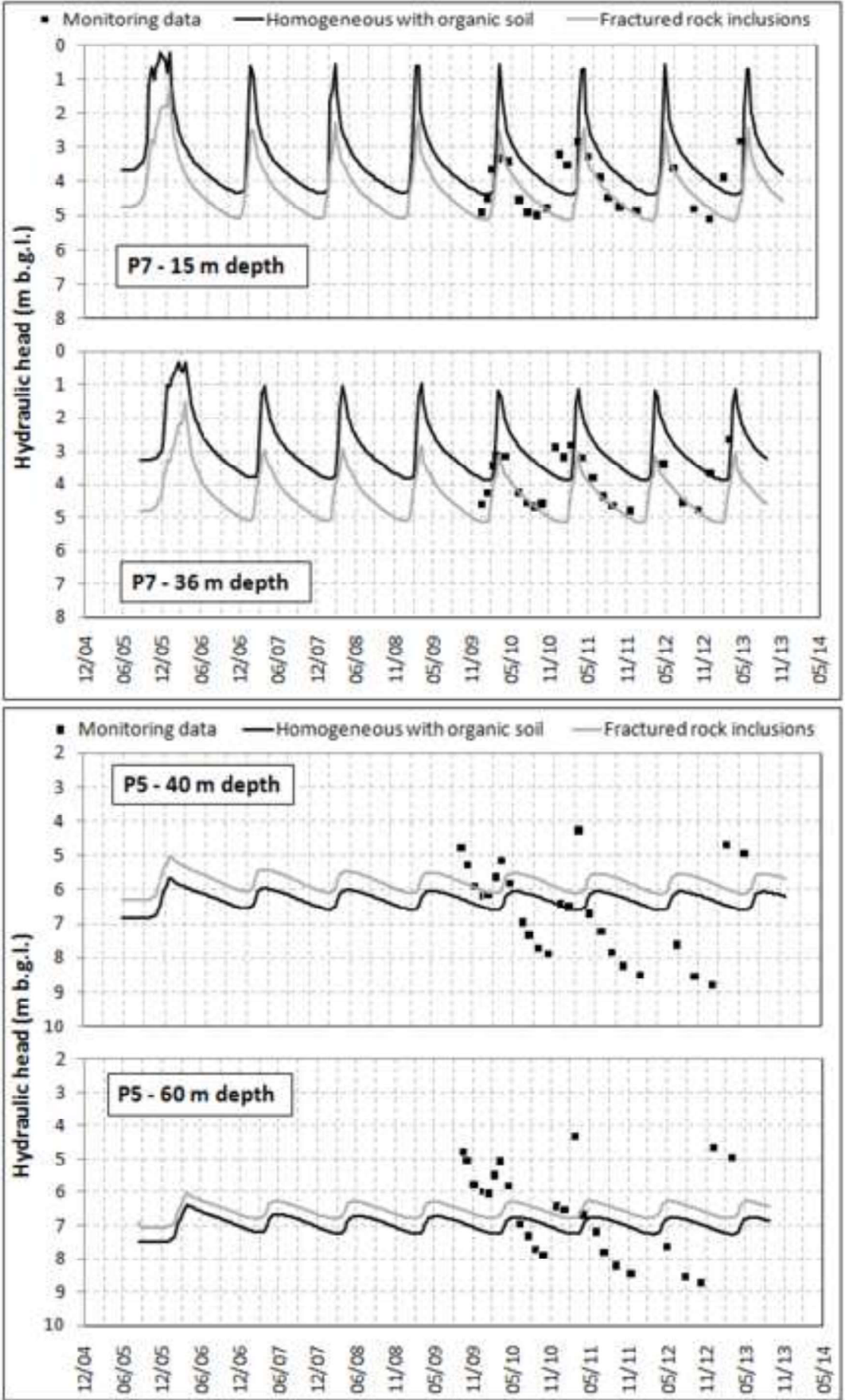


Table 2

[Click here to download Table: Table 2.pdf](#)

SOIL TYPE	SHEAR TEST RESULTS
SE scaly clay	$\phi'_{\text{peak}} \approx 18.5^{\circ}\text{-}20.5^{\circ}$ (<i>dry side</i> , $R \approx 3$) – (a) $\phi'_{\text{post-peak}} = 12^{\circ}\text{-}15^{\circ}$ – (a) $\phi'_{\text{r}} \approx 5^{\circ}$ – (b) $\phi^*_{\text{cs}} \approx 19^{\circ}$ – (a)
SCM scaly clay	$\phi'_{\text{peak}} \approx 13^{\circ}\text{-}22^{\circ}$ (<i>dry side</i> , $R \approx 2.5\text{-}20$) – (a) $\phi'_{\text{post-peak}} = 9^{\circ}\text{-}12^{\circ}$ – (a) $\phi'_{\text{r}} \leq 9^{\circ}$ – (c) $\phi^*_{\text{cs}} \approx 18^{\circ}$ – (a)
BENT	$\phi'_{\text{peak}} \approx 16^{\circ}\text{-}28^{\circ}$ (<i>dry side</i> , $R \approx 3\text{-}10$) – (a) $\phi'_{\text{post-peak}} = 12^{\circ}\text{-}27^{\circ}$ – (a) $\phi'_{\text{r}} \approx 5^{\circ}$ – (b) $\phi^*_{\text{cs}} \approx 16^{\circ}$ – (a)
PD1 and PD2 scaly clay	$\phi'_{\text{peak}} \approx 21^{\circ}\text{-}25^{\circ}$ (<i>dry side</i> , $R \approx 3\text{-}10$) – (a) $\phi'_{\text{post-peak}} = 13^{\circ}\text{-}20^{\circ}$ – (a) $\phi'_{\text{r}} \approx \text{n.d.}$ $\phi^*_{\text{cs}} \approx 18^{\circ}$ – (a)